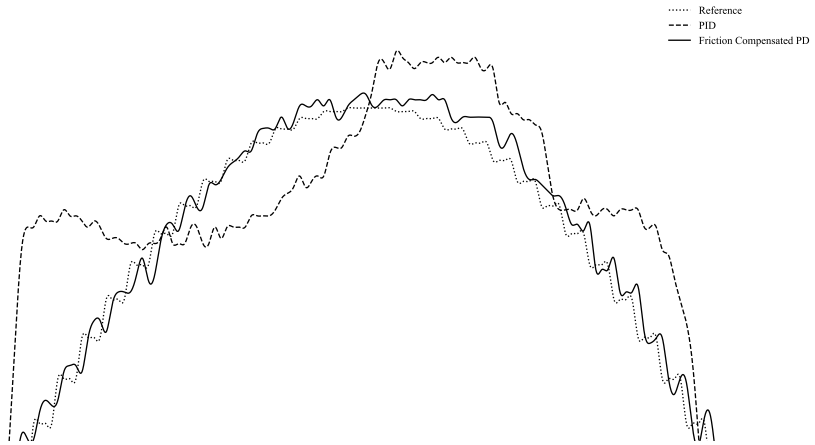

Friction Models and Friction Compensation for Real-Time Actuator Control

Master's thesis in Systems, Control and Mechatronics

JOHAN GUSTAFSSON
DENNIS HJERTÉN

DEPARTMENT OF ELECTRICAL ENGINEERING

CHALMERS UNIVERSITY OF TECHNOLOGY
Gothenburg, Sweden 2025
www.chalmers.se

Master's thesis 2025

Friction Models and Friction Compensation for Real-Time Actuator Control

JOHAN GUSTAFSSON
DENNIS HJERTÉN

CHALMERS
UNIVERSITY OF TECHNOLOGY

Department of Electrical Engineering
Division of Systems and Control
Examiner: Martin Fabian
Supervisor at T-Engineering: Emil Gustafsson
Chalmers University of Technology
Gothenburg, Sweden 2025

Friction Models and Friction Compensation for Real-Time Actuator Control

Supervisor: Emil Gustafsson, T-Engineering
Examiner: Martin Fabian, Head of Automation Research, Chalmers University of Technology

Master's Thesis 2025
Department of Electrical Engineering
Division of Systems and Control
Chalmers University of Technology
SE-412 96 Gothenburg
Telephone +46 31 772 1000

Cover: Position and reference collected from both a PID controller and a PD controller with friction compensation during a low velocity sine wave reference experiment.

Typeset in LaTeX
Printed by Chalmers Reproservice
Gothenburg, Sweden 2025

Abstract

Friction is a non-linear disturbance present in all electromechanical systems, which produces an opposing force or torque that resists motion. The effects become apparent and particularly problematic at low velocities, where the nonlinear friction characteristic reveals itself through phenomena such as limit cycles and stick-slip motion. This complex behavior presents significant challenges in high precision motion control systems. This thesis investigates methods for friction compensation in electromechanical actuators. Compensation strategies are implemented on an Engine Control Unit (ECU) which controls an Electronic Throttle Control (ETC) unit in real-time. Experimental results demonstrate that friction compensation techniques can significantly enhance the tracking performance and accuracy of the ETC at low velocities. Furthermore, the thesis highlights the trade-off between control signal activity and tracking performance, showing that different methods of compensation exhibit different characteristics in how they balance these objectives.

Keywords: Nonlinear Friction, Friction Compensation, Stick-slip motion, Limit cycles, Low-velocity control, Motion control, Electronic Throttle Control (ETC) unit, Engine Control Unit (ECU)

Acknowledgements

We would like to thank the Combustion and Transmission team at T-Engineering for their warm welcome and hospitality during our visit this spring. We would also like to extend a special thanks to our supervisor, Emil Gustafsson, who provided guidance throughout our whole work, and always took the extra time with us when we encountered roadblocks. We appreciate the insight into development of real-time control systems, an experience we will carry with us our whole careers.

Johan Gustafsson, Dennis Hjertén, Trollhättan, June 2025

Contents

List of Figures

List of Tables

1

Introduction

1.1 Background

Various electric servo actuators are used in automotive control systems, including applications such as electric power steering, wastegate control, Exhaust Gas Recirculation (EGR) valves, and Electronic Throttle Control (ETC) units. These actuators are used in modern combustion engine and automotive design as they enable precise regulation over variables such as air intake, exhaust flow, fuel delivery and steering angle [6]. These contribute to improved engine performance and fuel economy, lower emissions but also offer enhanced drivability by providing a more responsive and consistent feel to driver inputs [12].

All these electronic servo actuators experience non-linear friction, which presents control challenges, especially at low velocities, where high static friction must be compensated by the controller to achieve smooth and accurate reference tracking [1].

Friction has been referred to as a problem that is almost impossible to completely model [10]. It is non-linear, meaning that the static friction and dynamic friction can be very different, resulting in a behavior of sticking to a position and then quickly slipping to another position, known as stick-slip. It is also often asymmetrical, meaning that the control effort has to be different in the forward and backward direction of the actuator. To further complicate this issue, friction also depends on temperature and component aging [3].

The effect of friction and how to compensate for it in control systems has been researched for many years, and several important conclusions and advancements have been made [11]. While friction models have become further sophisticated, implementing them in real-time control systems also requires a balance between accuracy and computational simplicity. Research indicates that effective friction compensation has to be adaptive, meaning that the friction force must be continuously estimated and adjusted in real time, as it varies with temperature, wear and actuator dynamics [3].

In this thesis, the characteristics of time-invariant friction compensation methods are compared with those of adaptive friction compensation methods. Practical comparisons will be conducted on an Electronic Throttle Control (ETC) unit, demonstrating the methods performance in an experimental setting.

1.2 Aim

The aim is to investigate the key characteristics that differentiate the performance of different friction models and friction compensation methods when applied to a real-time controller.

1.3 Objectives

The objective is to analyze various friction models to identify the one that best captures the friction behavior of the electronic throttle control unit and is most suitable for integration into a real-time experimental controller. This involves evaluating the performance of various friction models by simulating them together with a plant and assessing their ability to replicate real-world friction characteristics. The most suitable friction model will be integrated into the controller to enhance the tracking performance by compensating for friction effects. Furthermore, another method of friction compensation called Active Disturbance Rejection Control (ADRC) will be evaluated and will therefore contribute with the comparison of adaptively compensating for disturbances like friction.

By comparing friction models within the context of a PID family-controlled throttle system, the study will explore adaptive and non-adaptive friction estimation techniques to determine their impact on control precision and stability. The findings will provide real world insights into selecting an optimal friction model that improves the responsiveness and tracking performance of the actuator.

2
Theory

2.1 Friction Modeling

Friction is the opposing force that occurs when two surfaces interact [11]. In the case of rotary actuators with gearboxes, there are several surfaces acting on each other, this can make the friction force great relative to the motor size.

Friction is often split into several parts, Coulomb friction which refers to a constant force independent of velocity. Dynamic friction which depends on velocity and static friction which is the force that needs to be overcome to initiate motion in the system. This force can be greater than the dynamic friction at low velocities, this is known as the Stribeck effect. The viscous friction, a linear dynamic friction force that increases with velocity is often not a problem in control systems as it can be compensated for quite easily and linearly [11].

The Stribeck effect can lead to a phenomenon known as stick-slip motion, the system will stick to a position until the driving force increases enough to overcome the static friction force, the friction force will then decrease as the systems velocity increases, until the system halts and the static friction force must be overcome again.

The friction force is often asymmetrical as it depends on which direction an actuator is moving. Friction also depends on environmental conditions such as temperature [3].

2.1.1 Dahl model

The Dahl model was introduced to capture friction in systems where elastic deformation occurs before sliding [11]. It is based on the stress-strain analogy from solid mechanics, where friction increases with displacement until reaching a limit force. The model is described by:

$$\frac{dF}{dx} = \sigma \left(1 - \frac{F}{F_c}\text{sgn}(v)\right)^{\alpha} \tag{2.1}$$

where F is the friction force, F_c is the Coulomb friction force, σ is the stiffness coefficient, and α is a shape parameter controlling the stress-strain curve.

While the Dahl model is simple and effective for simulating friction in bearings and servomechanisms, it does not capture stiction or the Stribeck effect, making it less accurate in applications where velocity-dependent effects are significant

2.1.2 LuGre model

The LuGre model, a friction model named after the cities Lund, Sweden, and Grenoble, France, referring to the research institutions where it was developed [4].

The LuGre model is a dynamic friction model developed to capture both static and dynamic friction behaviors. It was introduced as an extension of previous models, incorporating internal state variables to describe the microscopic deflections of asperities between two sliding surfaces. This model is particularly useful in control applications where accurate friction compensation is necessary [11].

The LuGre model represents friction as the interaction of elastic bristles at the contact interface, which bend and break as motion occurs. The average deflection of these bristles, denoted by the internal state variable z, is governed by the following differential equation:

$$\frac{dz}{dt} = v - \sigma_0 \frac{|v|}{g(v)} z, \tag{2.2}$$

where:

- v is the relative velocity between the two surfaces,
- σ_0 is the stiffness coefficient of the bristles,
- $g(v)$ is a function that characterizes the steady-state friction force.

The friction force is then given by:

$$F = \sigma_0 z + \sigma_1 \frac{dz}{dt} + \sigma_2 v, \tag{2.3}$$

where:

- σ_1 represents a damping coefficient that accounts for energy dissipation due to internal friction,
- σ_2 models the viscous friction component.

A key feature of the LuGre model is its ability to capture the Stribeck effect, which describes the decrease in friction force at low velocities before stabilizing at Coulomb friction levels. The function is typically chosen as:

$$g(v) = \alpha_0 + \alpha_1 e^{-(v/v_0)^2}, \tag{2.4}$$

where:

- α_0 is the Coulomb friction force,
- $\alpha_0 + \alpha_1$ is the static friction force,
- v_0 is the Stribeck velocity which determines the bounds of $\alpha_0 \leq g(v) \leq \alpha_0 + \alpha_1$.

The LuGre model successfully describes pre-sliding displacement, frictional lag, and varying break-away forces. Moreover, it has been widely used in control systems to implement friction compensation strategies. By estimating and compensating for the internal state variable z, precise motion control can be achieved, particularly in robotic actuators, servo mechanisms, and precision positioning systems.

Despite its advantages, the LuGre model has limitations. It does not inherently capture frictional memory effects observed in some experimental setups and may

require extensions to improve accuracy in highly dynamic applications. Variants of the model have been proposed to address these issues, including modifications that introduce additional state variables or alternative formulations of the damping term.

2.1.3 Continuously Differentiable Friction Model

It was proposed in [9] to use a continuously differentiable friction model (see Figure 2.1) suitable for high-performance control applications.

The proposed model is given by:

$$F_f(\dot{x}) = k_1(\tanh(l_1\dot{x}) - \tanh(l_2\dot{x})) + k_2 \tanh(l_3\dot{x}) + k_3\dot{x}, \tag{2.5}$$

where:

- k_1 and k_2 determine the static and Coulomb friction levels.
- l_1 and l_2 shape the Stribeck effect, which captures the drop in friction at low velocities.
- l_3 governs the transition to steady-state Coulomb friction.
- k_3 represents the coefficient of viscous friction.

This model effectively captures key friction phenomena such as the Stribeck effect, Coulomb friction, and viscous damping while remaining continuously differentiable. The smooth transitions between different friction regimes make it particularly advantageous for control applications, as it avoids the instability issues associated with discontinuous models.

Despite its benefits, the model assumes symmetric friction behavior and may require extensions to account for directional asymmetries or hysteresis effects observed in some real-world applications.

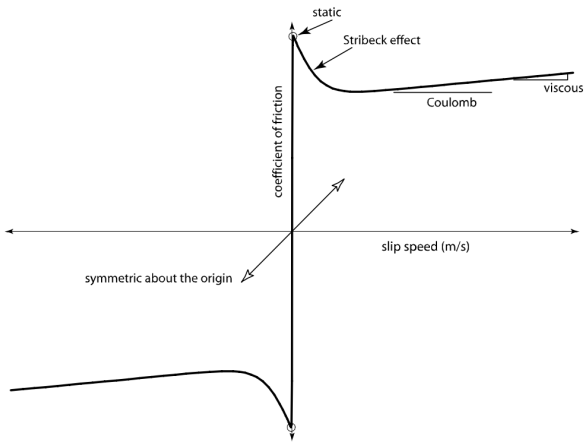

Figure 2.1: Characteristics of the continuously differentiable friction model taken from [9].

2.2 Electronic Throttle Control (ETC) Unit

The Electronic Throttle Control (ETC) unit is an actuator that plays an important role in the control of most modern combustion engines. It controls the airflow into the engine, thus influencing the air-fuel mixture and the engine's combustion process by moving a throttle plate using a DC motor. The ETC solves many problems that the cable actuated throttle used in earlier engine control designs had. It allowed much easier implementation of functions such as cruise control and idle air control, also reducing cost as the individual actuators for these functions or the cable linkage was not needed. Furthermore, it allows functions such as adaptive driving modes like sport and comfort by simply changing the relationship between pedal and throttle position. It also allows enhanced driver feel as load changes or gear changes can be compensated for by the ETC [7].

An ETC is mainly comprised of a throttle plate, housing, DC motor, reduction gears and a position sensor [8]. Its function is to electronically control the throttle plate angle according to the calculated angle from accelerator pedal position and driver assistance systems. A simplified schematic of the ETC layout is shown in Figure 2.2.

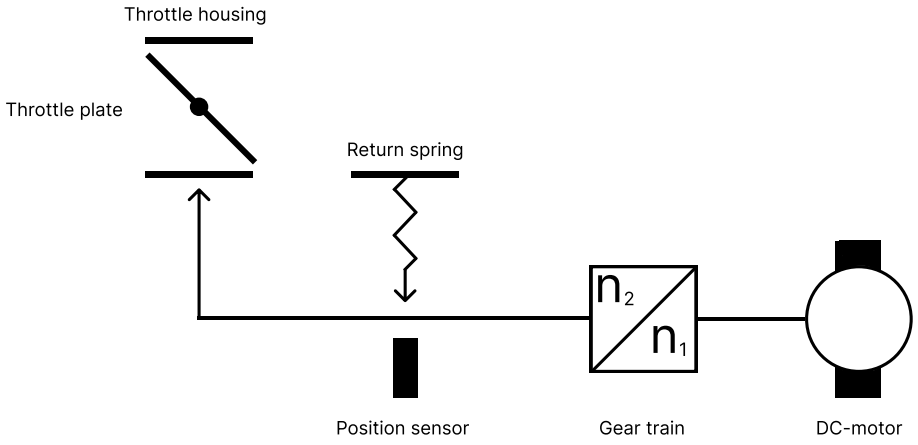

Figure 2.2: Simplified schematic of the ETC unit showing the DC motor, gear train, position senor, return spring, throttle plate, and housing.

The system consists of a DC motor driving a gear train, which in turn controls the throttle plate, A position sensor monitors the axle's angle, while a return spring returns the throttle plate to its limp home position (LHP). The LHP is located such that the throttle plate is a few degrees open so as to ensure some air flow even in the case of breakdown. A second return spring is therefore used to bring the throttle plate from completely closed to the limp home position. The throttle housing is also equipped with mechanical stops in the fully closed, zero degrees position and the fully opened, 90 degrees position.

The DC-motor can be modeled as

$$V = Ri + L\frac{di}{dt} + K_e\omega, \tag{2.6}$$

where V is the voltage applied to the motor armature, R is the armature resistance, i is the motor current, L is the motor inductance, $\frac{di}{dt}$ is the change in current with respect to time, K_e is the electromotive force constant of the motor and ω is the angular velocity.

The torque can be described by

$$J\dot{\omega} = K_t i - T_f - T_s. \tag{2.7}$$

Here J is the total moment of inertia of the system, K_t is the motor torque constant, i is the motor current, T_f is the friction torque, which is a function of ω, and T_s is the spring torque.
A comprehensive representation of the plant model used in the control architecture is given in Figure 2.3.

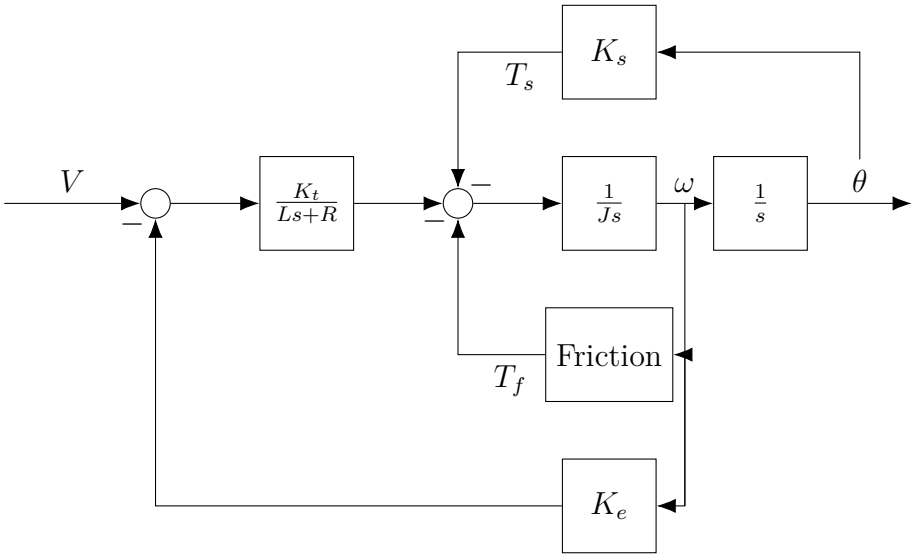

Figure 2.3: The schematic diagram of the throttle control unit.

2.3 Feed Forward with Friction Model

Feedforward control is used to enhance system performance by anticipating and compensating for known disturbances and system dynamics. In scenarios where frictional and elastic forces significantly influence system behavior, incorporating their estimated effects into the control input improves trajectory tracking accuracy and mitigates steady-state errors.

In the present work, the feedforward control component is formulated to offset the expected frictional and elastic torques acting upon the system. By applying the required compensation torque in advance, the controller reduces reliance on feedback mechanisms, thereby enabling more precise motion control.

As the friction is a function of velocity, it is necessary to construct a reference velocity signal. This reference velocity is generated based on the error between the desired and the actual position, which is r_ω in Figure 2.4. Subsequently, a proportional-derivative (PD) controller is used to compensate for the velocity tracking error.

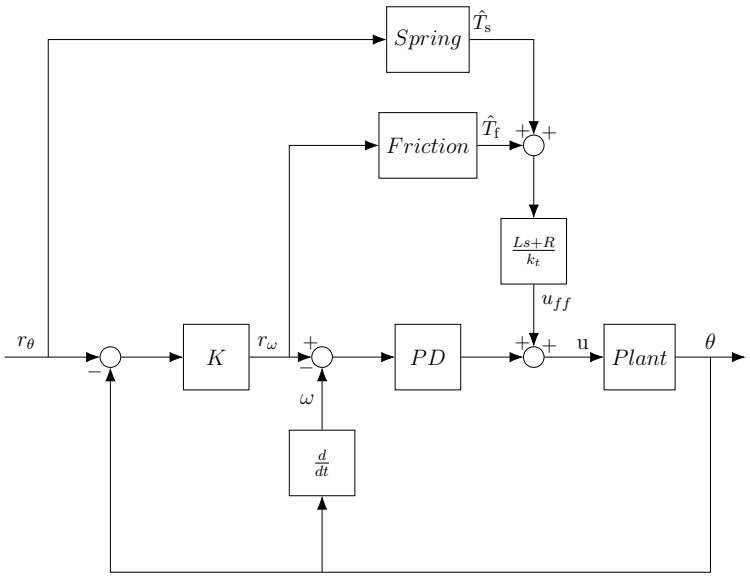

Figure 2.4: PD scheme with additional spring and friction compensation.

Given that the control input is in the form of voltage, while the friction and elastic compensations are defined in terms of torque, it is essential to transform the feedforward torque into an equivalent voltage command. Hence the term $\frac{Ls+R}{k_t}$ in Figure 2.4 which is the inverse of the first block in the plant, as can be seen in Figure 2.3. The total feedforward voltage is expressed as:

$$u_\mathrm{ff} = \frac{(\hat{T}_\mathrm{f} + \hat{T}_\mathrm{s})(Ls + R)}{k_t}, \tag{2.8}$$

where $\hat{T}_\mathrm{f}$ denotes the estimated frictional torque and $\hat{T}_\mathrm{s}$ represents the estimated elastic (Spring in Figure 2.4) restoring torque.

2.4 Active Disturbance Rejection Control

Active Disturbance Rejection Control (ADRC) is a control scheme that has been used to compensate for several different kinds of disturbances, linear and nonlinear, inluding friction. Friction compensation using an ADRC controller was studied in [2] for a bi-axis servo system and in [13] for a tank gun control system. A linear ADRC controller was implemented in [5] to control an electronic throttle control unit to compensate for non-linearities including friction.

The ADRC controller can be linear using a linear extended state observer (ESO) and error feedback. It can also be modified to be non-linear using a non-linear ESO and non-linear state error feedback. This thesis will study the characteristics of friction compensation using a linear ESO coupled with both linear and non-linear state error feedback.

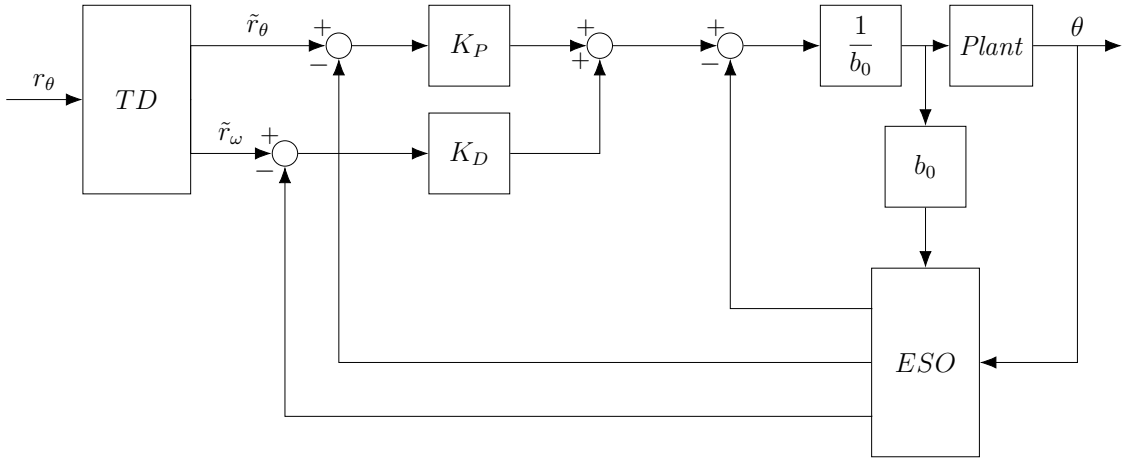

Figure 2.5: ADRC Controller scheme.

The linear ADRC scheme is illustrated in Figure 2.5. It contains three main components, the Tracking Differentiator (TD), the linear state error feedback, and the linear Extended State Observer (ESO).

The TD generates a smoothed reference position trajectory $\tilde{r}_\theta$ and its derivative, the reference velocity trajectory $\tilde{r}_\omega$. These reference signals are used in the state error feedback controller, which applies the proportional gain K_P and the derivative gain K_D to compute the control signal. The position and velocity states of the system are estimated along with the total estimated disturbance by the ESO.

The effect of the plant's critical input gain is accounted for by introducing the inverse of the estimated input gain $\frac{1}{b_0}$. This allows the separation of the control signal derived from the state feedback from the total disturbance estimated by the ESO, ensuring effective disturbance rejection and improved control performance.

2.4.1 Tracking Differentiator

The Tracking Differentiator (TD) is a key component of an Active Disturbance Rejection Control (ADRC) structure. Its purpose is to generate a smooth and

realizable reference position signal out of the potentially noisy and abrupt input reference position signal while also differentiating the reference position signal and generating a reference velocity signal.

This Tracking Differentiator is implemented as a linear second-order system defined by:

$$\begin{bmatrix} \dot{x}_1 \\ \dot{x}_2 \end{bmatrix} = \begin{bmatrix} x_2 \\ \dfrac{r - x_1 + x_2(T_1 - T_2)}{T_1 T_2} \end{bmatrix}, \tag{2.9}$$

where:

- x_1 is the smooth output reference position;
- x_2 is the generated reference velocity;
- T_1 and T_2 are the time constants that determine the response characteristics.

The time constants T_1 and T_2 are tuned for system performance. T_2 can be adjusted to achieve the desired rise time, while T_1 controls the damping of the system. The state-space representation in Equation 2.9 is transformed into a second-order system by applying the Laplace transform, as shown in the following equations. Here, $X_1(s)$ and $R(s)$ represent the Laplace transforms of x_1 and the reference signal r, respectively.

$$s^2 X_1(s) = \frac{R(s) - X_1(s) + sX_1(s)(T_1 - T_2)}{T_1 T_2} \tag{2.10}$$

$$s^2 X_1(s) T_1 T_2 = R(s) - X_1(s) + sX_1(s)(T_1 - T_2) \tag{2.11}$$

$$X_1(s)(s^2 T_1 T_2 - s(T_1 - T_2) + 1) = R(s) \tag{2.12}$$

$$G(s) = \frac{X_1(s)}{R(s)} = \frac{\dfrac{1}{T_1 T_2}}{s^2 - \dfrac{T_1 - T_2}{T_1 T_2} s + \dfrac{1}{T_1 T_2}} \tag{2.13}$$

Compare to standard second order system:

$$G(s) = \frac{\omega_n^2}{s^2 + 2\zeta\omega_n + \omega_n^2}. \tag{2.14}$$

Comparing the second order system in (2.13) and the tracking differentiator Laplace function in (2.14), it follows that:

$$\frac{1}{T_1 T_2} = \omega_n^2, \text{ and } -\frac{T_1 - T_2}{T_1 T_2} = 2\zeta\omega_n. \tag{2.15}$$

The time constant T_2 is therefore a function of T_1 if the system is critically dampened, that is, when $\zeta = 1$:

$$T_2 = \frac{T_1^{\frac{3}{2}} \pm \sqrt{T_1^3 + 8}}{2\sqrt{T_1}} \tag{2.16}$$

3
Methods

3.1 Hardware and experimental setup

The experimental setup consists of a host PC which runs the control algorithms and sends command signals via a CAN bus interface, connected to an Electronic Control Unit (ECU). The ECU communicates with an Electronic Throttle Control (ETC) unit, which serves as the actuator in the control system. A regulated power supply provides the necessary electrical power to the ECU.
An illustration of the hardware used in the experiments can be seen in Figure 3.1.

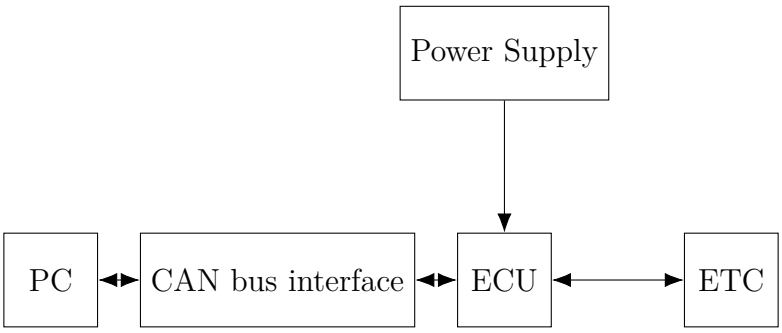

Figure 3.1: The schematic diagram of the experimental setup.

3.2 Plant Modeling

This section outlines the modeling approach for the DC motor and the experimental methods that will be used to analyze its friction behavior. The primary objective is to develop a model that will accurately replicate the system's real-world position response in simulation, in order to determine which friction model most effectively captures the system's behavior.

3.2.1 DC Motor Parameter Estimation

To achieve an accurate representation of the DC motor dynamics, parameter estimation will be performed with the goal of aligning the simulated position with the experimentally measured position. A high-frequency excitation signal, specifically a *chirp* signal (a signal which changes frequency over time, which can be seen in Figure 4.1), will be used to excite the motor across a broad frequency range while

avoiding complete stops in motion. This approach will minimize the influence of static friction, allowing the estimation process to focus on dynamic parameters.

Motor resistance and inductance will be measured directly using an LCR meter to provide initial values. The remaining parameters, including the back-emf constant and viscous friction (damping) coefficients, will be tuned using least-squares estimation based on measured velocity and position responses. The estimated parameters will then be validated by comparing the simulated position trajectory against experimental data, with the aim of minimizing discrepancies between the two.

The parameters will be systematically varied, individually increased and decreased, and validated using the least squares method to determine whether the updated values reduce the error between the measured and simulated position. If an improvement is observed, the updated value is adopted as the new parameter. This process is repeated iteratively until no further changes lead to a reduction in the least squares error.

3.3 Friction Model Evaluation

After identifying the baseline motor parameters, additional experiments will be conducted to evaluate different friction models. The focus of this evaluation will be to determine which model most accurately reproduces the real system's position response, particularly under conditions where static friction plays a significant role.

3.3.1 Simulating High Static Friction

To amplify the effects of static friction, experiments will be designed where the applied input (torque, voltage, or current) is gradually increased while the system remains stationary until motion is initiated. This setup will allow for the observation of static friction thresholds and the transition from sticking to sliding motion.

The recorded position trajectories from these experiments will serve as a reference for validating the friction models. The goal will be to match the simulated position to the experimental position as closely as possible, particularly in regions affected by stick-slip phenomena.

3.3.2 Comparative Evaluation of Friction Models

Three friction models will be evaluated:

- Dahl Model
- LuGre Model
- Continuously Differentiable Friction Model

Each model will be implemented within the simulation, and its parameters will be adjusted with the same experimental method as in plant parameter estimation where the mean square error(MSE) will be the metric used.

The model achieving the lowest error in the MSE between the simulated and measured position will be selected for integration into the control design.

3.4 ADRC Tuning

The ADRC Controller has five tunable parameters:

b_0	Input gain approximation
T_1, T_2	Time constants of the Tracking Differentiator
ω_o	Observer bandwidth
ω_c	Controller bandwidth

Table 3.1: Tunable parameters of the ADRC Controller

3.4.1 Estimation of Input Gain b_0

The linear first order system from input signal to angular velocity can be described by the equation below, where $\dot{y}$ is the angular velocity, u is the input signal and $f(t)$ is the total disturbance, which includes unknown dynamics and other disturbances:

$$\dot{y} = b_0 u + f(t). \tag{3.1}$$

From Figure 3.2 we get that for a step in DC from 0% to 15% the angular velocity increase with 99.23, with a sampling time of 10ms. From this the critical gain b_0 can then be calculated accordingly:

$$a = \frac{\Delta Y}{\Delta t} \tag{3.2}$$

$$b_0 = \frac{a}{u} \tag{3.3}$$

$$b_0 = \frac{\Delta Y}{u \Delta t} = \frac{99.23}{15 \cdot 0.010} \approx 661.5. \tag{3.4}$$

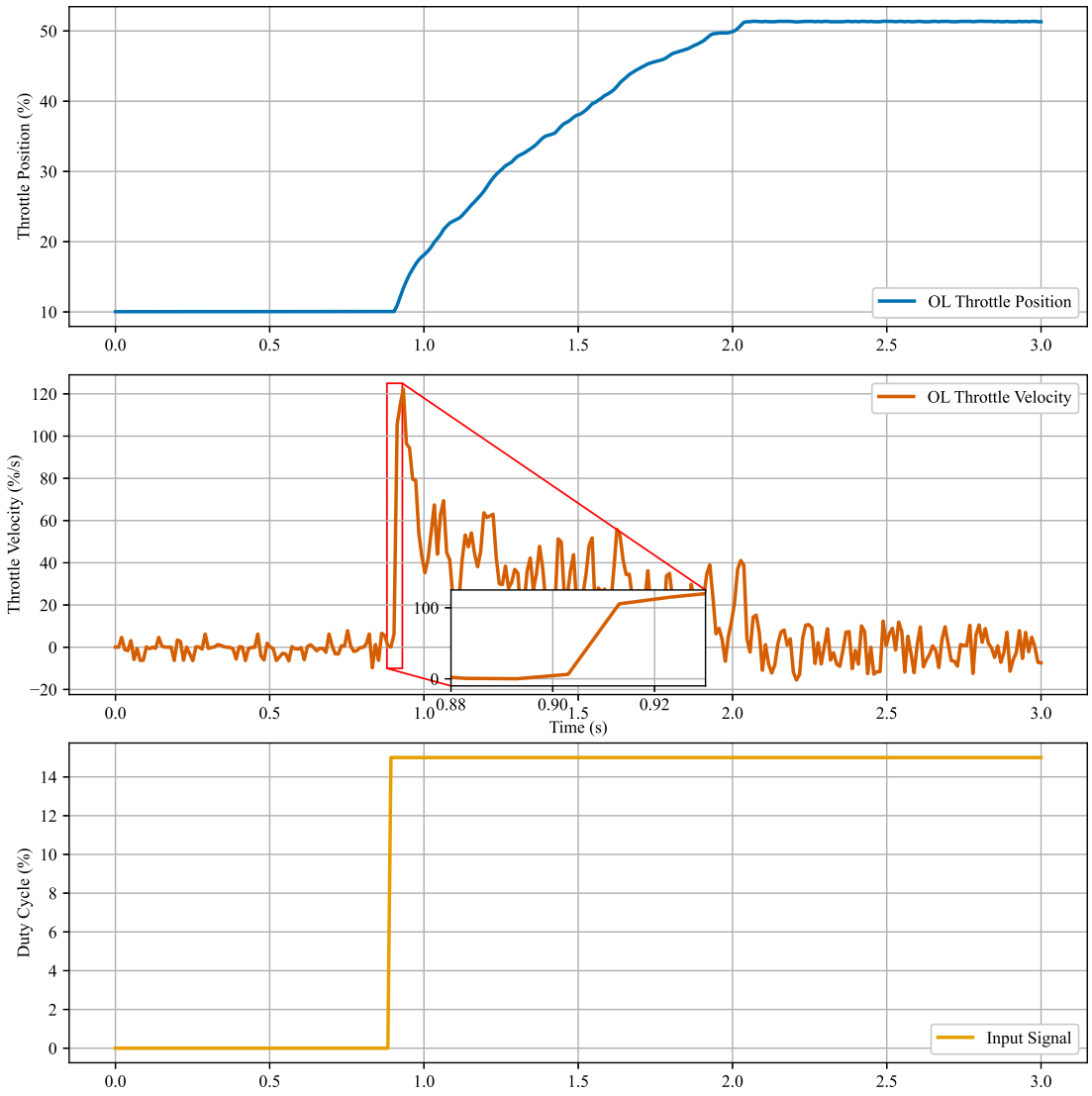

Figure 3.2: Angle and angular velocity response to an open-loop input step.

3.4.2 Tracking Differentiator (TD) Tuning

The Tracking Differentiator (TD) has two tunable parameters, T_1 and T_2, whose relationship is defined by (2.16). As a result, only one of these parameters needs to be tuned directly, while the other can be determined from their relationship.

For reference, a controller previously developed by T-Engineering, referred to as the T-PID, is available. The TD will be tuned to achieve a response time similar to that of the T-PID controller. By matching the TD's settling time to that of the T-PID, the system is ensured to reach the reference within a proven and feasible time frame.

The tuning process is based on a step response experiment, where the reference is increased from 20 to 30. The TD parameters are adjusted such that the system's response closely aligns with the T-PID's performance under this test condition.

3.4.3 Extended State Observer (ESO) Tuning

A key parameter in tuning the Extended State Observer (ESO) is the observer bandwidth ω_o. This parameter determines how quickly the observer estimates the system states and the total disturbance. A higher observer bandwidth enables faster disturbance rejection but may amplify measurement noise, while a lower bandwidth reduces sensitivity to noise at the expense of slower response.

A common guideline for selecting ω_o is to set it larger than the controller bandwidth ω_c, typically in the range of 3 to 5 times ω_c.

In practice, ω_o is initially selected conservatively to avoid excessive noise amplification. It is then incrementally increased during testing while monitoring the estimated states and the control input. The tuning process seeks the highest ω_o that provides sufficiently fast and accurate disturbance estimation without introducing unacceptable levels of noise or instability.

3.4.4 Linear controller tuning

The controller bandwidth ω_c is tuned together with the observer bandwidth ω_o, ensuring that the observer bandwidth is set to at least twice the value of the controller bandwidth. The controller for the Electronic Throttle Control (ETC) unit is tuned empirically by evaluating its ability to accurately track the reference signal through iterative testing and analyzing its performance. A too low controller bandwidth results in sluggish reference tracking which leads to the observer interpreting the tracking error as an external disturbance, misleading the disturbance rejection mechanism. Setting the controller bandwidth too high leads to excessive sensitivity to noise but also decreases tracking performance if it is so high that the observer is not able to converge fast enough. The controller will then react to inaccurate state estimations from the observer, offering inaccurate and delayed reference tracking.

Through iterating the process of increasing the controller bandwidth and observing controller performance, it was found for low values ($\omega_c = 50$ to 80) that the controller was unable to efficiently track the already set trajectory of the Tracking Differentiator (TD). Increasing the value from 80, the controller's reference tracking performance is increased as well as its sensitivity to noise. The values $\omega_c = 90$ to 100 was deemed sufficient. Increasing the values would offer higher control signal activity without any meaningful increase to tracking performance. An increase in noise within the control signal is undesirable, particularly because the control strategy is being applied to an ETC unit. Excessive noise can lead to unnecessary actuator wear and mechanical stress and it is therefore not considered feasible to control the system with an overly aggressive and noisy signal.

Two controller tuning configurations were selected for investigation. The first used bandwidths of $\omega_c = 100$ rad/s and $\omega_o = 340$ rad/s, maximizing tracking performance. The second configuration with $\omega_c = 95$ rad/s and $\omega_o = 260$ rad/s, initially demonstrated comparable performance while significantly reducing noise in the control signal.

3.4.5 Nonlinear controller tuning

To address key limitations observed in the linear controller, a nonlinear controller was developed as an alternative to the linear designs. Firstly, the return spring in the ETC unit requires significantly greater control effort when opening the throttle compared to closing it. This asymmetry challenged the linear controller's ability to maintain consistent performance across the operating range. Additionally, the linear controller struggled with large reference step changes in both directions and showed greater control signal noise than other methods. The nonlinear controller was developed to better handle these nonlinear characteristics and improve robustness.

The nonlinear controller gain was implemented using a one-dimensional interpolated lookup table. The input to the table is the error between the reference signal prior to the Tracking Differentiator and the actual position of the throttle plate. Based on the magnitude of this error, the lookup table dynamically returns the corresponding controller bandwidth ω_c. This enables the controller to adjust its responsiveness in real time and the gain can be adjusted to combat the mentioned challenges with the constant gain. The gain table was empirically tuned and iteratively adjusted for all the mentioned challenges in the different scenarios. Firstly, lower bandwidth was set for small errors to reduce control signal noise, mainly when the system is at a halt. Secondly, the gain for the biggest errors could be lowered to combat the overshoot present when applying great reference step changes. Thirdly, the added robustness from the gain being lowered in the small and high magnitudes of the error allowed the moderate error magnitude to be increased, yielding a faster system at moderate reference step changes. Lastly, the gain could be lowered when closing the throttle, as the return spring already significantly moves the throttle plate in the closing direction. The lookup table values are given in Figure 3.3 and Table 3.2.

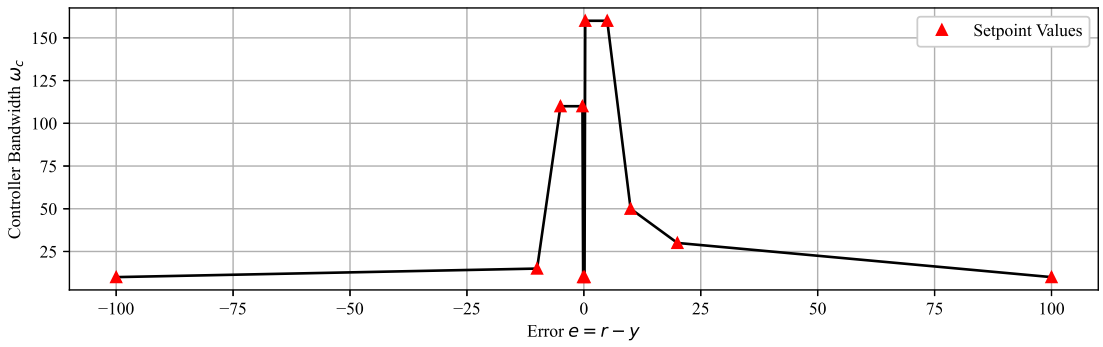

Figure 3.3: Visualization of the Lookup table for the controller bandwidth ω_c.

ω_c	10	15	110	110	10	10	160	160	50	30	10
Error	-100	-10	-5	-0.3	-0.15	0.15	0.3	5	10	20	100

Table 3.2: Lookup table for the controller bandwidth ω_c.

4
Results

4.1 Parameter Estimation

In this section, the experimental results will be presented, with a primary focus on developing a model that can accurately replicate the system's measured position response. The process will involve estimating the DC motor parameters and evaluating different friction models based on how well they enable the simulated position to match the experimental position. Multiple friction models will be compared to assess their ability to reproduce the system's behavior, and the model that achieves the closest match will be selected for integration into the feedforward controller design, as described in Section 2.3.

4.1.1 DC Motor Parameter Estimation

To estimate the DC motor parameters, an open-loop *chirp* signal was applied in the form of a sinusoidal waveform. The frequency of the signal increased linearly from 0.6 Hz to 4 Hz over a duration of 120 seconds, while the duty cycle varied between 0% and 20%. The chirp signal corresponds to the duty cycle shown in Figure 4.1.

While R and L where conducted by the use of an LCR-meter, the rest of the parameters where systematically updated to achieve the lowest possible MSE between the simulated and actual position, the final parameters are set as follows:

R	3
L	$1.2 \cdot 10^{-3}$
k_t	$1.2 \cdot 10^{-4}$
k_e	$1.2 \cdot 10^{-4}$
J	$7.7 \cdot 10^{-8}$

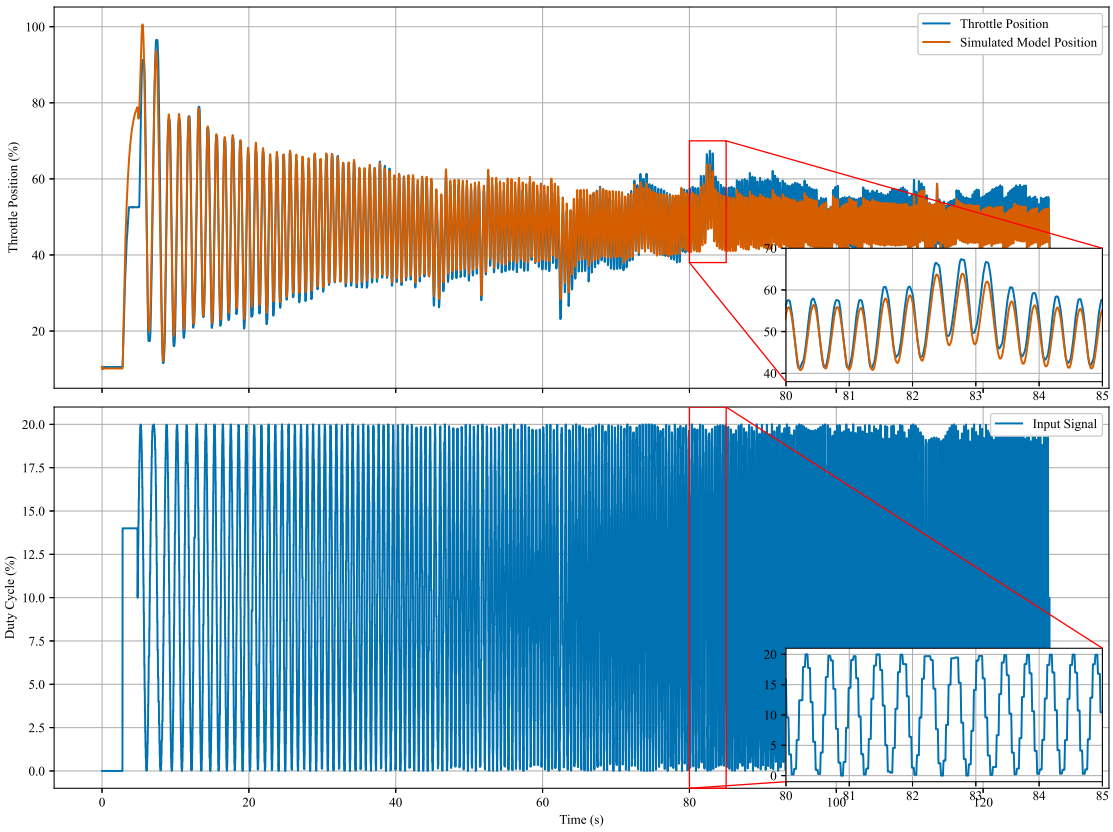

Figure 4.1: Comparison of estimated and actual throttle position for the DC motor.

4.1.2 Comparison of Friction Models

The system exhibits significant static friction (see Figure 4.2), which negatively impacts the accuracy of the Dahl model compared to the other two friction models that incorporate static friction effects.

The friction estimation experiment consists of step responses, sinusoidal and *chirp* input signals. Between these steps, the duty cycle is gradually increased to capture static friction effects, followed by an increase and decrease in duty cycle while maintaining a constant throttle position. The input signal can be seen in Figure 4.2.

4.1.2.1 Dahl Model

By using the MSE between the actual and simulated position as a metric to systematically change the parameters for the Dahl model, the estimated parameters are as follows, with a MSE of 259.37:

σ	$3.17 \cdot 10^{-8}$
F_c	$9.28 \cdot 10^{-4}$
α	17.09

The final result when using the Dahl model is seen in Figure 4.2, where there is significant static friction at approximately $t = 230$, where the duty cycle increases slowly to 10% and then decreases while the position remains nearly the same. The Dahl model is unable to capture this behavior effectively, leading to a high MSE.

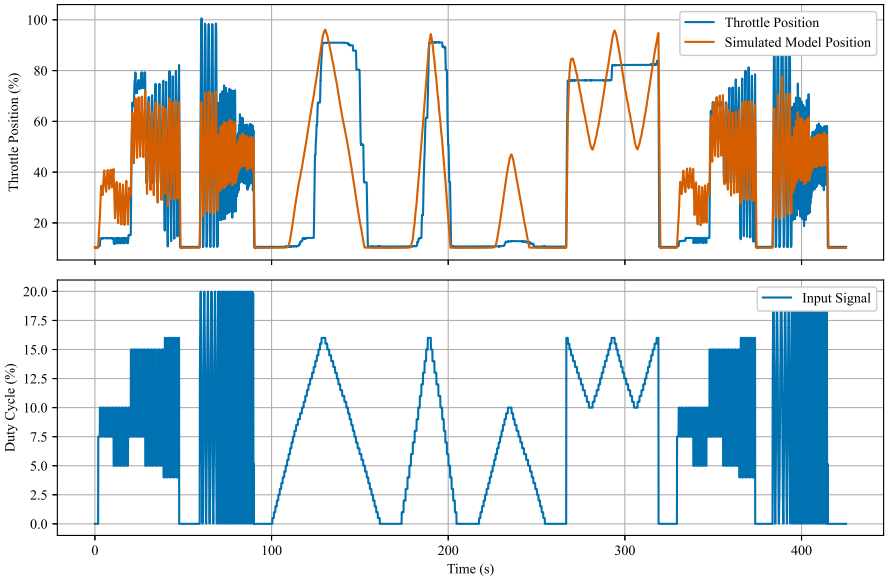

Figure 4.2: Friction estimation experiment for the Dahl model.

4.1.2.2 Continuously Differentiable Friction Model

Just as the Dahl model the parameters where estimated with the goal of minimizing the MSE between the actual and simulated position. For the continuously differentiable friction model the final parameters are as follows, with the MSE of 49.50.

k_1	$1.43 \cdot 10^{-4}$
k_2	$8.72 \cdot 10^{-5}$
k_3	$2.03 \cdot 10^{-6}$
l_1	328.57
l_2	1.33
l_3	$1.45 \cdot 10^{4}$

Compared to the Dahl model, the continuously differentiable model captures static friction effectively, as can be seen in Figure 4.3. However, certain discrepancies remain in accurately modeling the real friction behavior.

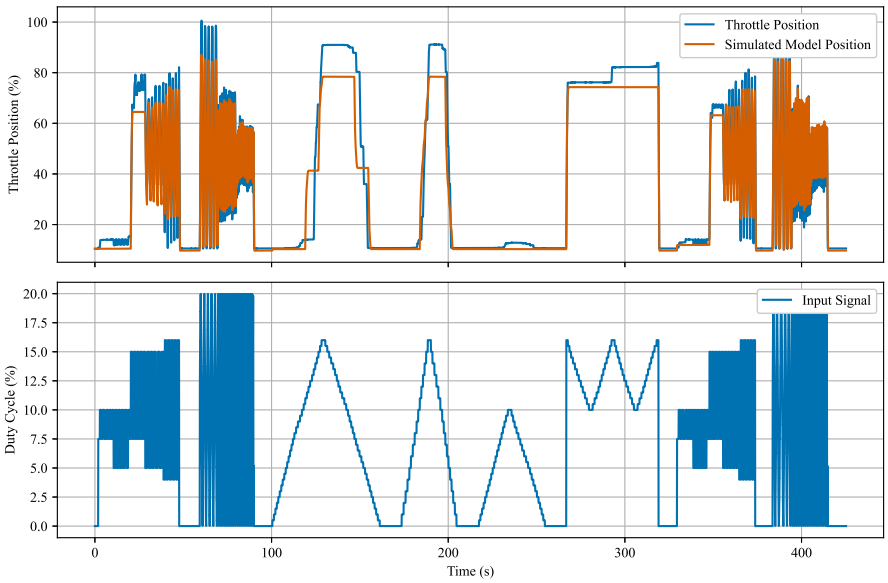

Figure 4.3: Friction estimation experiment for the continuously differentiable model

4.1.2.3 LuGre Model

As the previous experiment the parameters where made to minimize the MSE between the actual and simulated position. The estimated parameters for the LuGre model are as follows with a MSE of 26.42:

σ_0	$3.52 \cdot 10^{-5}$
σ_1	$2.15 \cdot 10^{-3}$
σ_2	$2.50 \cdot 10^{-6}$
α_0	$8.27 \cdot 10^{-6}$
α_1	$7.05 \cdot 10^{-4}$
v_0	$1.45 \cdot 10^{4}$

The LuGre model effectively captures static friction and demonstrates superior performance, as can be seen in Figure 4.4. As indicated by the MSE values, the LuGre model achieves a lower error compared to the continuously differentiable model, suggesting a more accurate representation of the friction dynamics in the system.

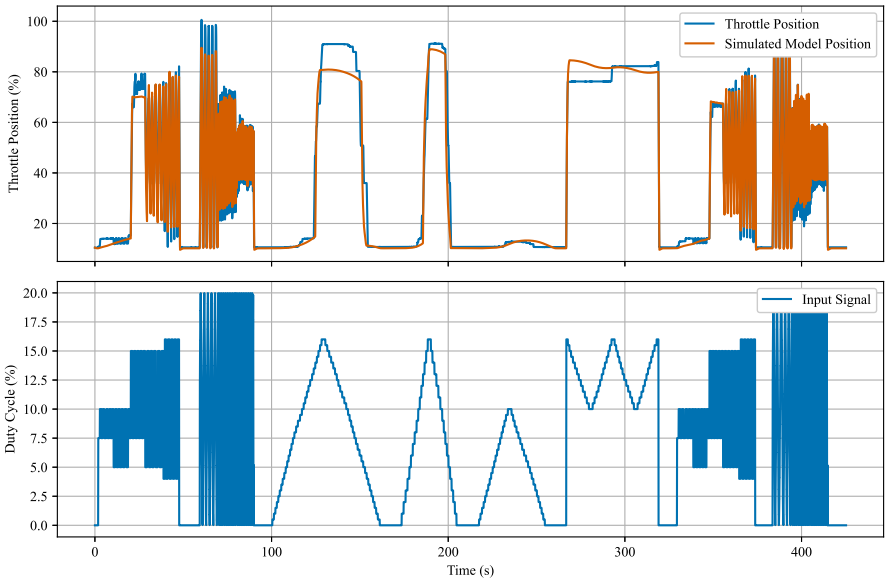

Figure 4.4: Friction estimation experiment for the LuGre model

4.2 Comparison of controllers

In this section, each controller will be evaluated starting with a PID controller without any form of friction compensation. This initial evaluation serves to highlight the necessity of incorporating friction compensation.

Following this, two linear ADRC controllers will be compared to assess whether increasing the control and observer bandwidths provides any performance benefit. The most suitable linear ADRC controller from this comparison will then be evaluated against a non-linear ADRC controller. The more promising of these two will be selected for the final experiment.

The final experiment involves a comparison between the best-performing ADRC controller, a feedforward friction compensating controller, and the proprietary controller developed by T-Engineering.

All controllers will be evaluated based on the following performance metrics:

- Mean squared error (MSE) between the reference and actual position,
- Rise time (defined from 0% to 95% of the reference step),
- Overshoot,
- Variance in control activity.

The selection of the most suitable ADRC controller will be based on these metrics, with a primary focus on achieving a fast system response while minimizing control activity.

Four different test scenarios are used to evaluate the performance of each controller:

- A step response from 20% to 30% in the reference position, both without and with a -10% load disturbance applied to the final control signal.
- A ramping reference starting from the Limp Home Position (LHP), increasing up to 100%, and then returning to LHP.
- A low-frequency sine wave oscillating between 20% and 70%, with a -10% load disturbance applied, followed by a $+10\%$ disturbance.
- A reference impulse from 20% to 90%, both without and with a -10% load disturbance applied to the final control signal.

While all the controllers are evaluated on these tests, the PID without friction compensation is only evaluated on the ramping and sine wave test, mainly beacuse that is where the frictional force is mostly effecting the system.

4.2.1 PID Control without Friction Compensation

The first controller that will be looking into is a PID controller without any friction compensation where we can see the effect of stick slip motion in Figure 4.5 and Figure 4.6. When comparing this controller with a controller that has friction compensation in the sinusoidal experiment (see Figure 4.17) it can be observed that the stick slip motion is compensated for.

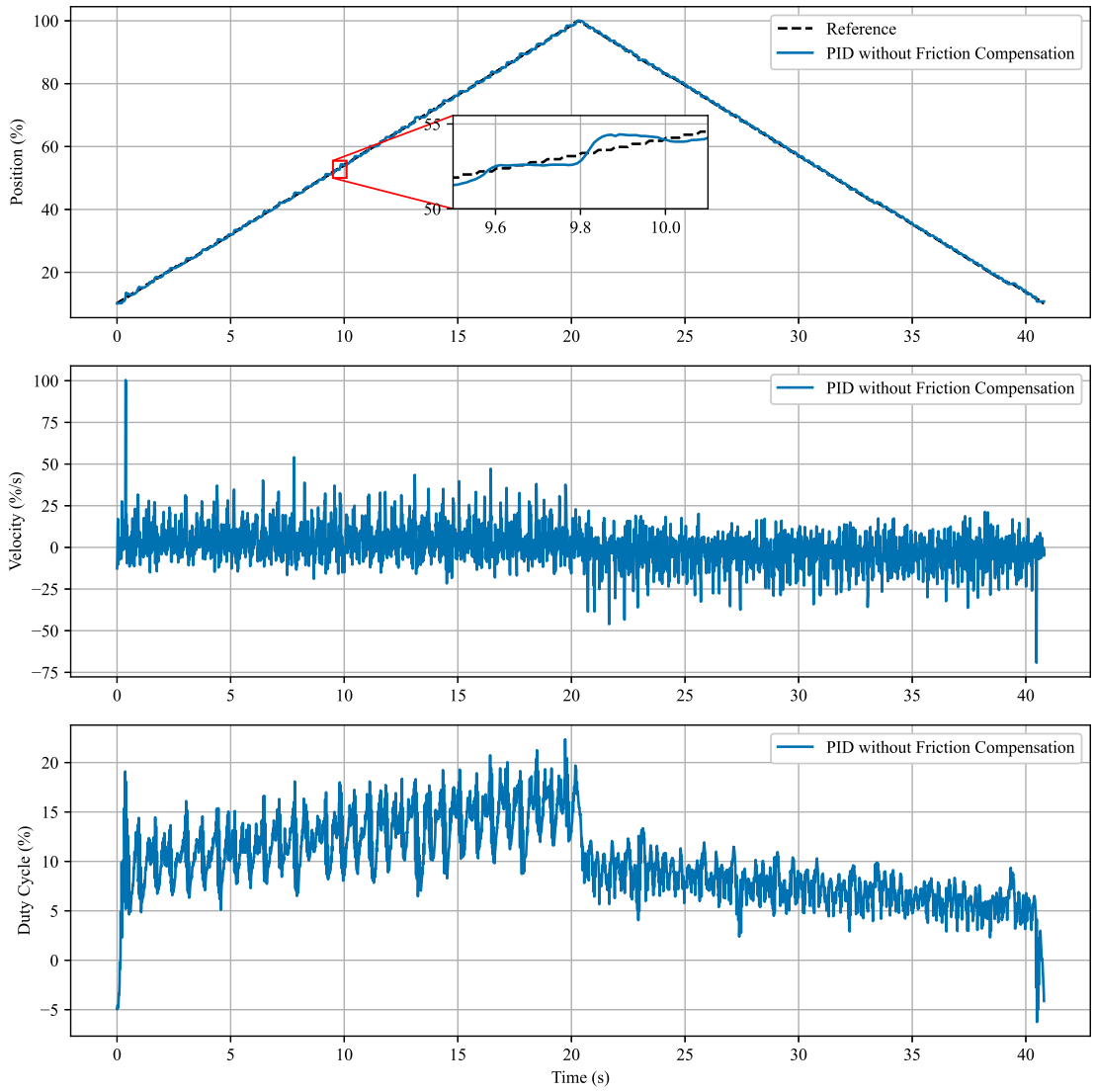

Figure 4.5: PID Controller without Friction Compensation, Response for Ramping Reference (LHP-100-LHP).

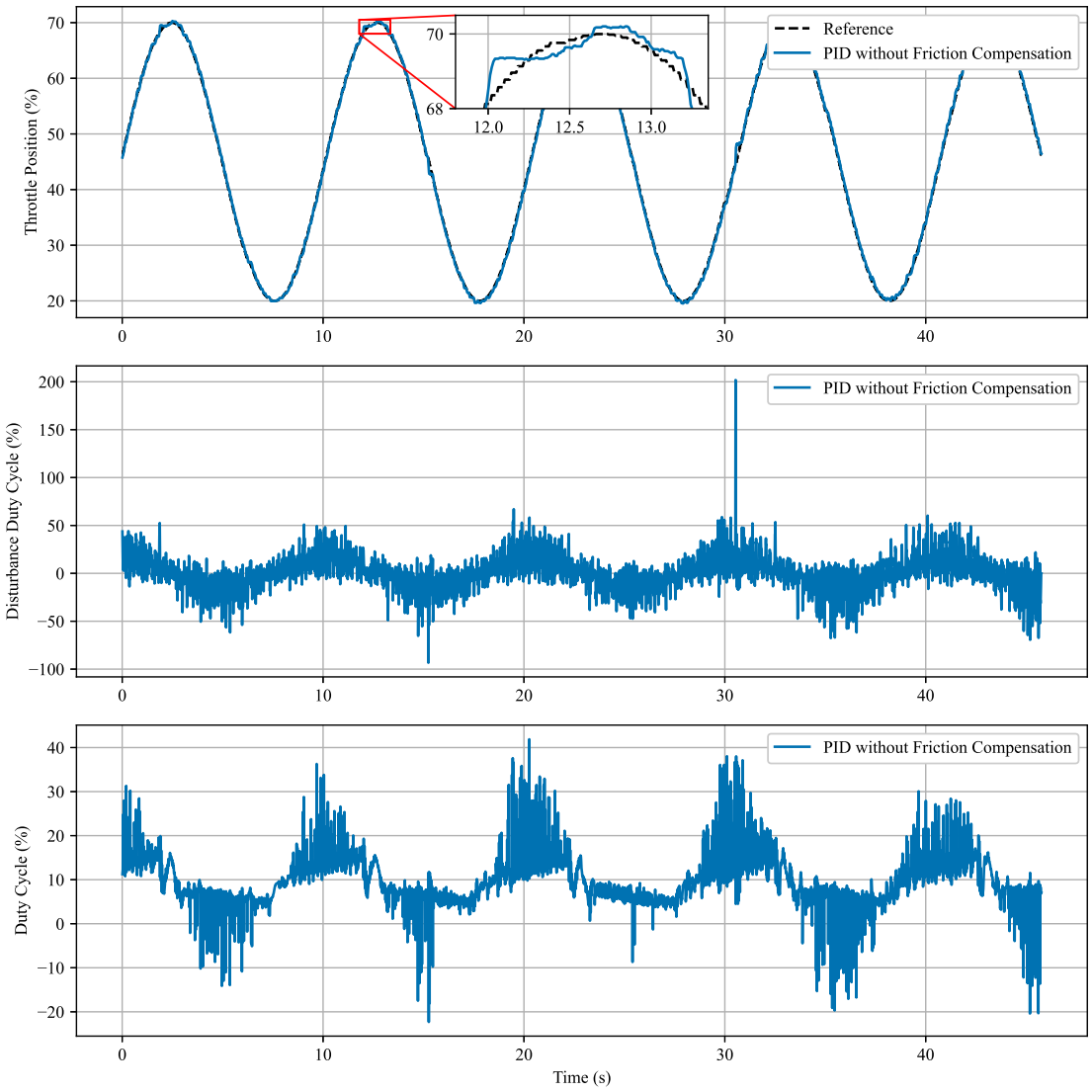

Figure 4.6: PID Controller without Friction Compensation, Tracking on Sine Wave with Load Disturbance added.

4.2.2 Real-Time ADRC Implementation on ECU

4.2.2.1 Comparison between Linear ADRC controllers

Two different linear ADRC controller tunings were evaluated and their corresponding step responses between 20% and 30% are shown in Figure 4.7. A 10% duty cycle decrement is made to the final control signal before the step in the right column of the figure to represent a load disturbance to the system.

C1: Control bandwidth $\omega_c = 100$ rad/s and observer bandwidth $\omega_o = 340$ rad/s.
C2: Control bandwidth $\omega_c = 95$ rad/s and observer bandwidth $\omega_o = 260$ rad/s. In addition, a low-pass filter with a coefficient of 0.45 was applied to the control signal in C2.

The low-pass filter was implemented using a function from T-Engineering's MATLAB library. The filtered input is computed as,

$$u_i = u_c \cdot \lambda + u_{i-1} * (1 - \lambda), \tag{4.1}$$

where u_i is the input applied to the system, u_{i-1} is the previous input value, u_c is the controller output and λ is the low-pass filter coefficient.

Figure 4.7 shows a step response from 20% to 30% duty cycle. In the plots on the right, an additional disturbance of -10% duty cycle is applied to evaluate the controller's performance under load. As can be observed in Table 4.1 from the damped control signal of Controller C2, the controller gains can be reduced without causing an overshoot greater than 1% or extending the step response time between 20% and 30% beyond 100 ms. Additionally, this reduction in gains significantly decreases steady-state noise in the control signal, which is evident from the duty cycle behavior shown in the two lower plots of the figure.

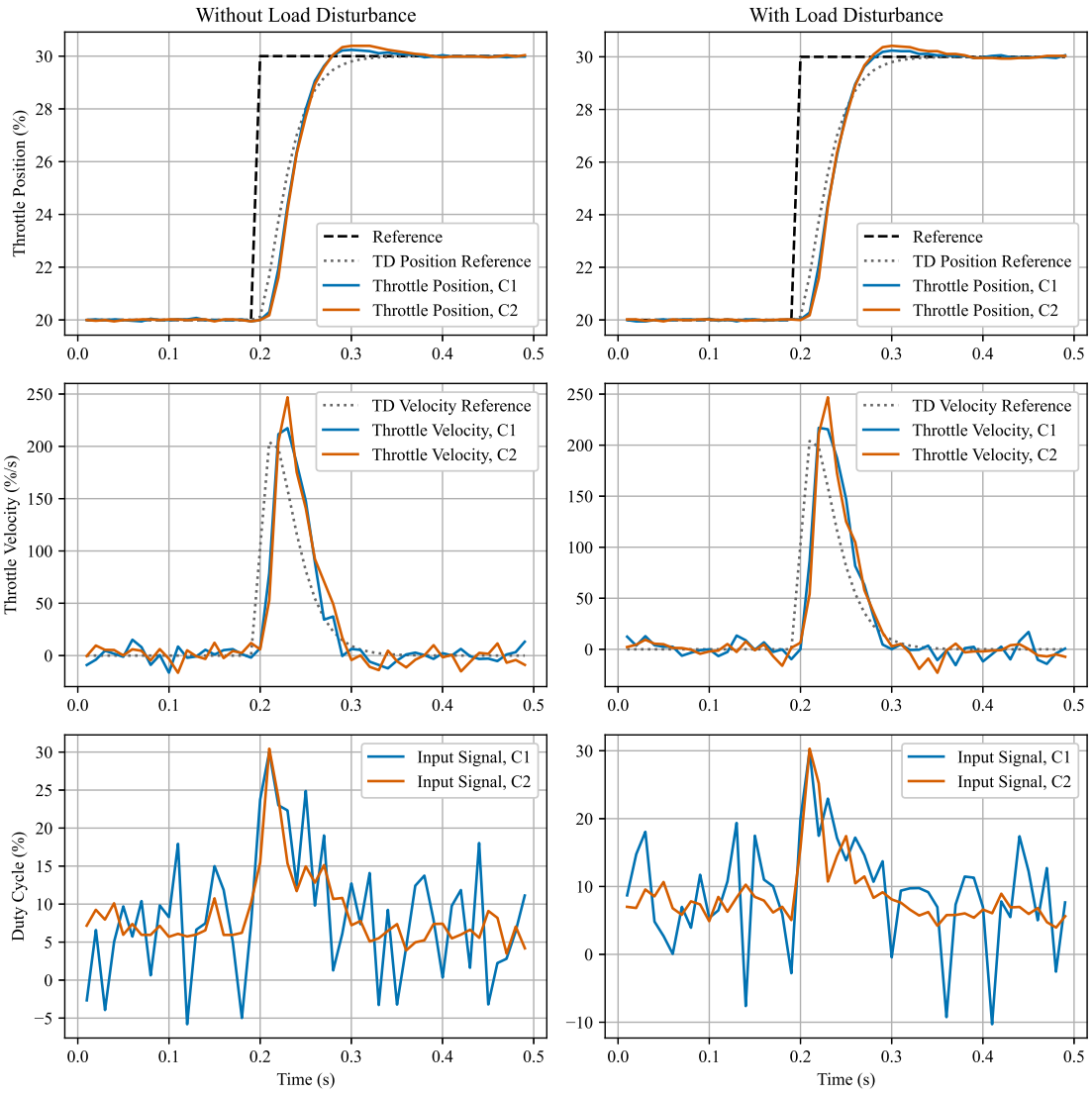

Figure 4.7: Comparison of Step Response between 20% and 30% of ADRC Controllers C1 and C2, with and without Load Disturbance

In Figure 4.8 there is ramping reference from the Limp Home Position (LHP), up to 100%, and back down to LHP. In Table 4.3 it can be observed that the dampened controller, C2, perform similarly to C1 but with a decrease in control signal activity in steady state.

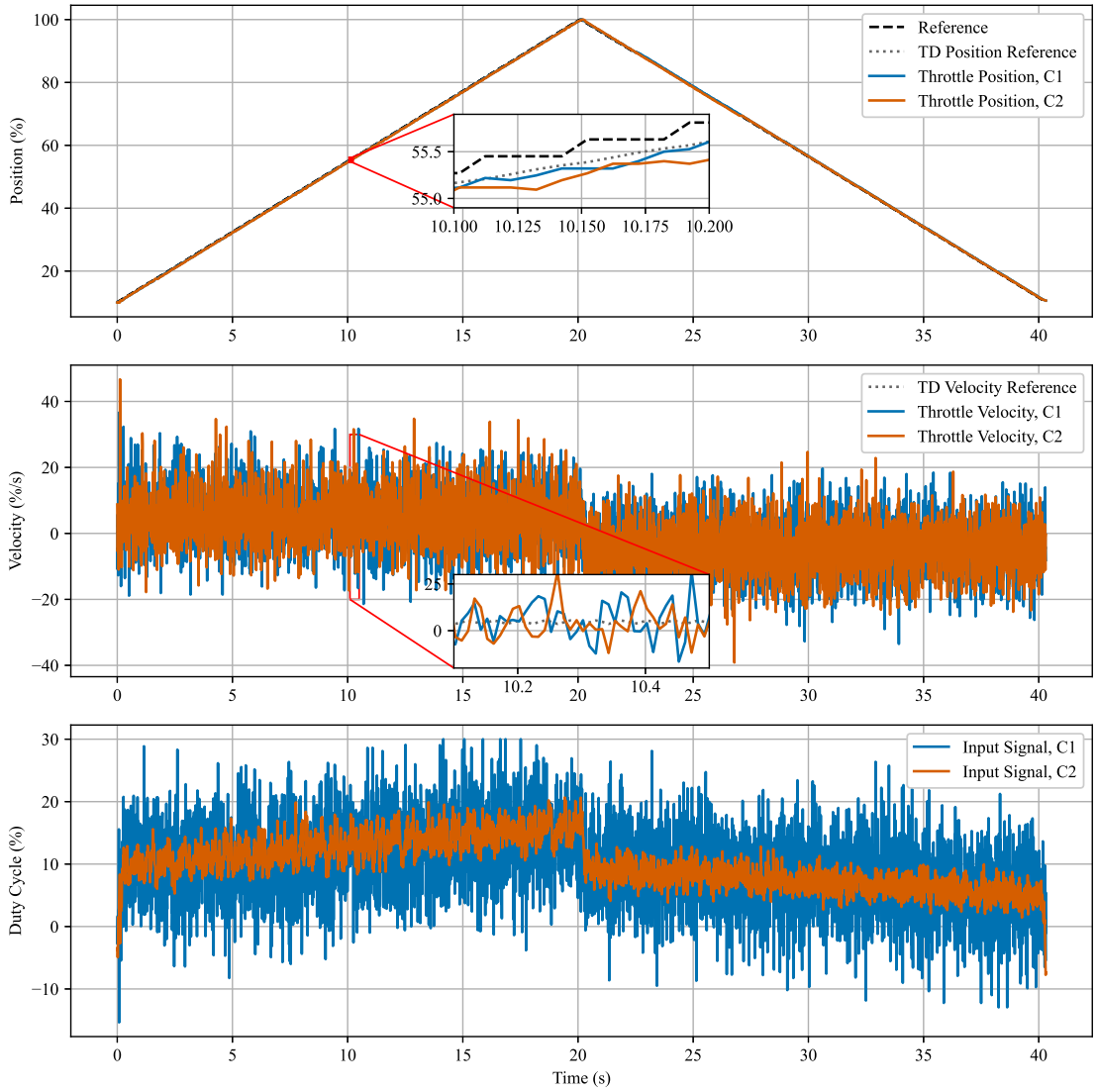

Figure 4.8: Comparison of ADRC Controllers C1 and C2, Response for Ramping Reference (LHP-100-LHP).

The low-velocity tracking performance and the controllers disturbance rejection ability is evaluated for both controller tunings using a low frequency sine wave from 20% to 70% in Figure 4.9. A load disturbance is applied to the final control signal according to the figure. It can be observed in Table 4.4 that it is the same case as the experiment before that they controllers perform similarly but the C2 controller uses less control activity.

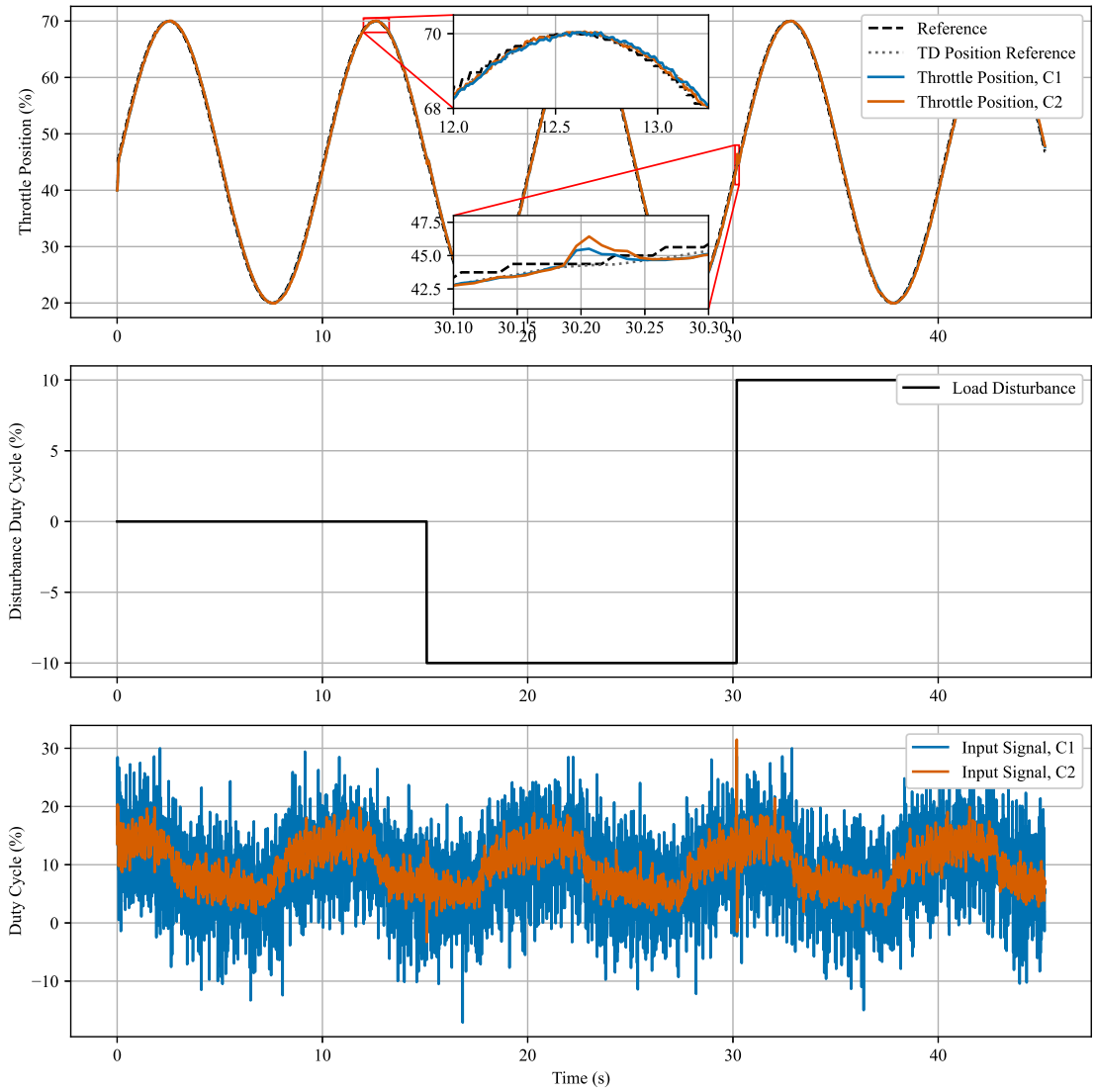

Figure 4.9: ADRC Controllers C1 and C2, Tracking on Sine Wave with Load Disturbance added.

The controllers performance across the operating range is evaluated by applying a reference impulse from 20% to 90%, as shown in Figure 4.10. A load disturbance of -10% duty cycle is applied before the reference step shown in the right column of the figure. Just as the previous experiments between C1 and C2 the both controllers perform similarly but the control activity is for C2 is decreased. What can be observed is that the duty cycle in both experiments are clamped at 95% and -35% due to how T-Engineering has set as the max and min control signal to not excite the hardware too much.

But what is extra important here is that in both cases when the reference goes from 90% to 20% both controllers undershoot so much that they hit the mechanical stop at 0%. This undershoot is what lead to the non-linear controller bandwidth ω_c which will be evaluated next.

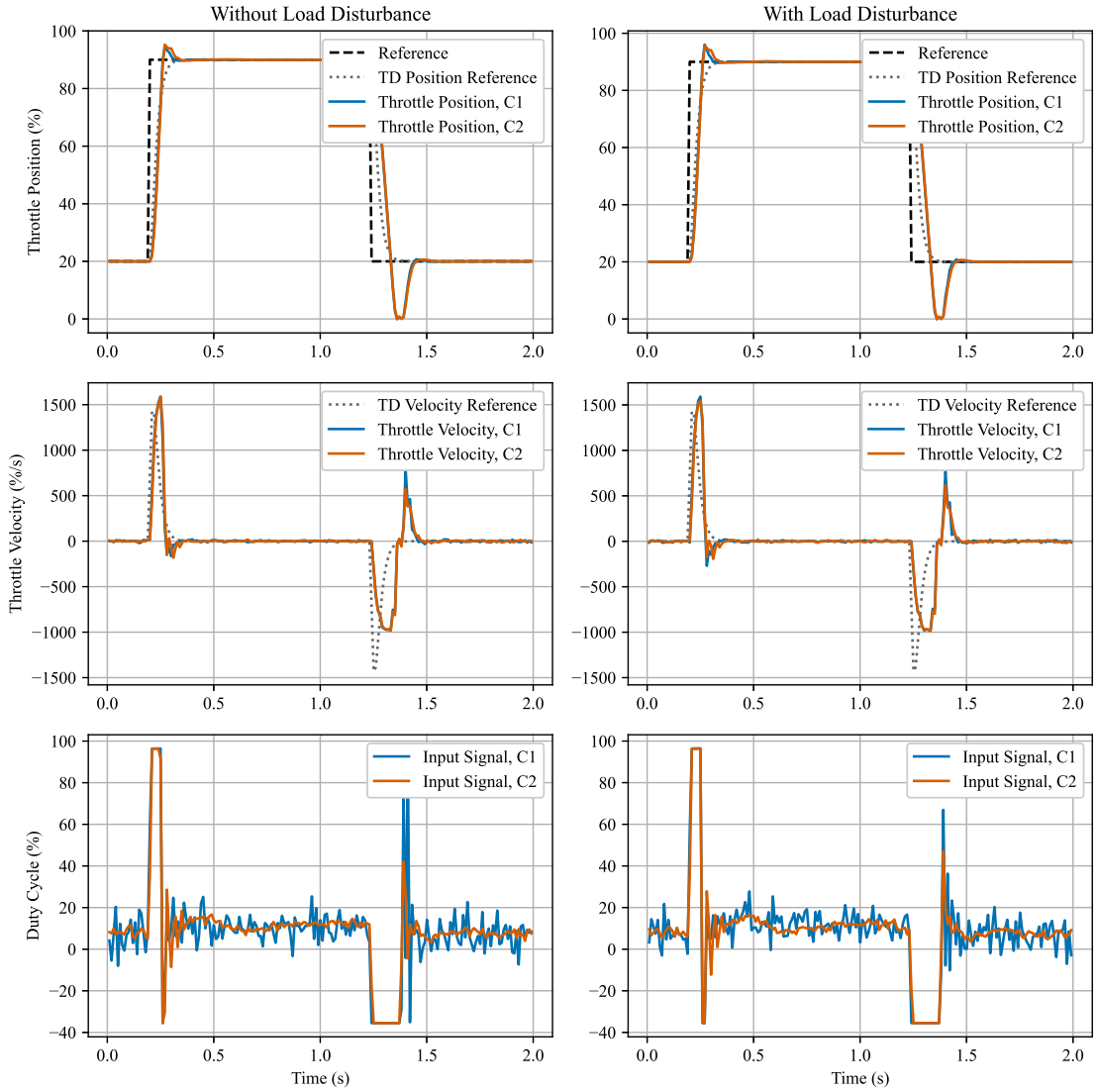

Figure 4.10: Comparison of Impulse Response between 20% and 90% of ADRC Controllers C1 and C2, with and without Load Disturbance.

4.2.2.2 Comparison between Linear and Non-Linear ADRC Controllers

A nonlinear ADRC controller(C3) is compared to the linear ADRC controller C2. Their step responses between 20% and 30% were evaluated as shown in Figure 4.11. Here, the load disturbance in the right column is a -10% in duty cycle.

C2: Control Bandwidth $\omega_c = 95$ rad/s and observer bandwidth $\omega_o = 260$ rad/s with a low-pass filter with coefficient 0.45 applied to the control signal.

C3: Control bandwidth is a nonlinear function of the error between the reference and position and observer bandwidth $\omega_o = 260$ rad/s. An illustration of the controller bandwidth ω_c can be seen in Figure 3.3 and the numerical values is shown in Table 3.2

Here we see the both controllers perform similarly in the response time and the overshoot. But what is most important is that in the steady state the nonlinear ADRC has a lower control activity which can be seen in the lower row in the figure.

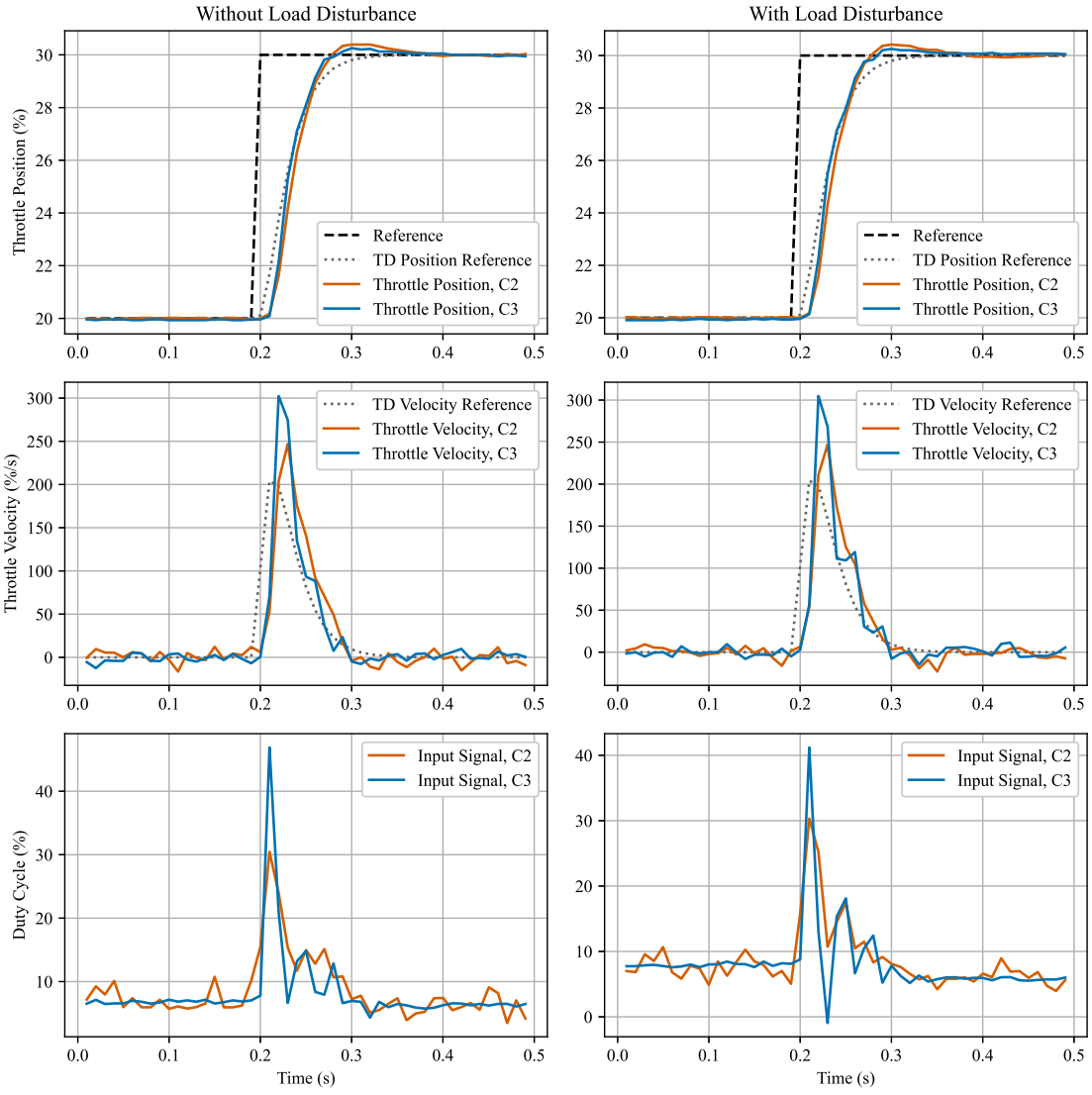

Figure 4.11: Comparison of Step Response of ADRC Controllers C2 and C3, with and without Load Disturbance

The low-velocity tracking performance and the controllers ability to handle the full operating range are evaluated in Figure 4.12 for both controllers using a ramping reference from LHP up to 100%, and back down to LHP.

In this experiment it can be observed in Table 4.3 that the nonlinear ADRC performs slightly worse when comparing the reference to the position, however there is a decrease in control activity which is desirable.

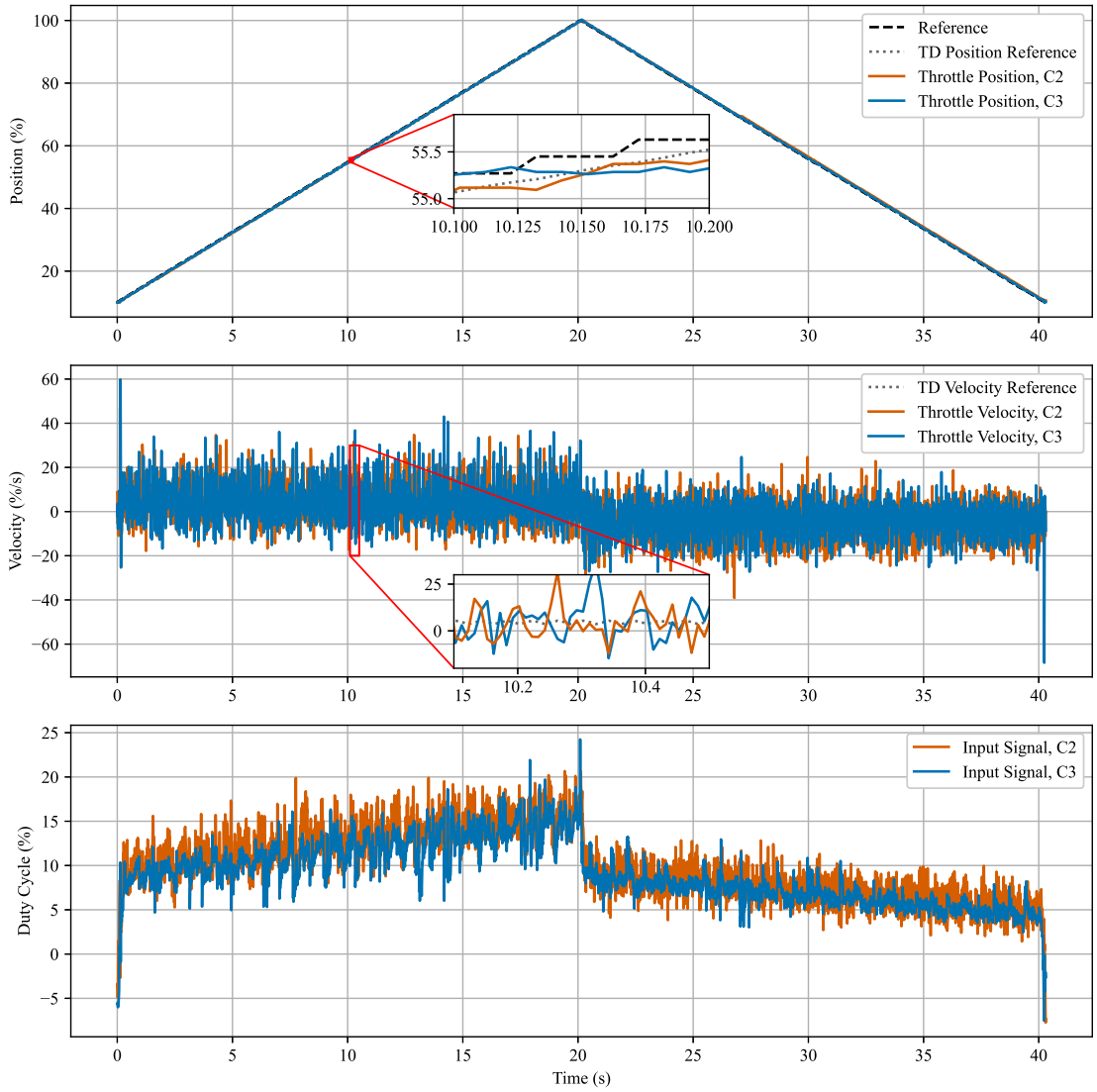

Figure 4.12: Comparison of ADRC Controllers C2 and C3, Response for Ramping Input (LHP-100-LHP)

The low-velocity tracking performance and the controllers disturbance rejection ability is evaluated for both controllers using a low frequency sine wave from 20% to 70% in Figure 4.13. A load disturbance is applied to the final control signal according to the figure.

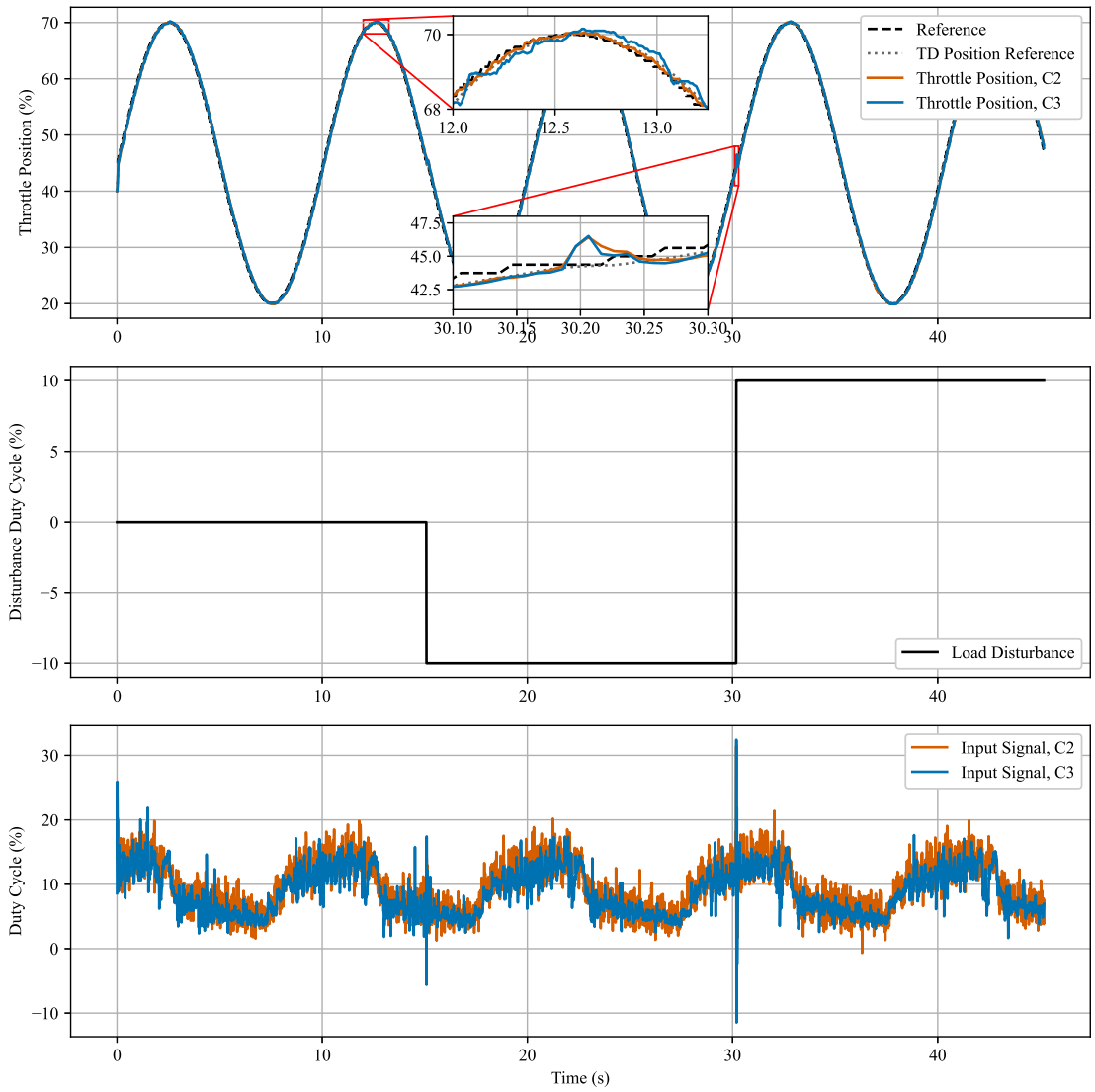

Figure 4.13: ADRC Controllers C2 and C3, Tracking on Sine Wave with Load Disturbance added

The controllers performance across the operating range is evaluated by applying a reference impulse from 20% to 90%, as shown in Figure 4.14. A load disturbance of −10% duty cycle is applied to the final control signal before the reference step shown in the right column of the figure.

Here it can be observed that the nonlinear ADRC has a slightly smaller overshoot during the rise of the impulse. In the fall of the impulse there is no undershoot from the nonlinear ADRC, while the linear ADRC undershoots down to the mechanical stop at 0%, which was main reason for the nonlinear implementation.

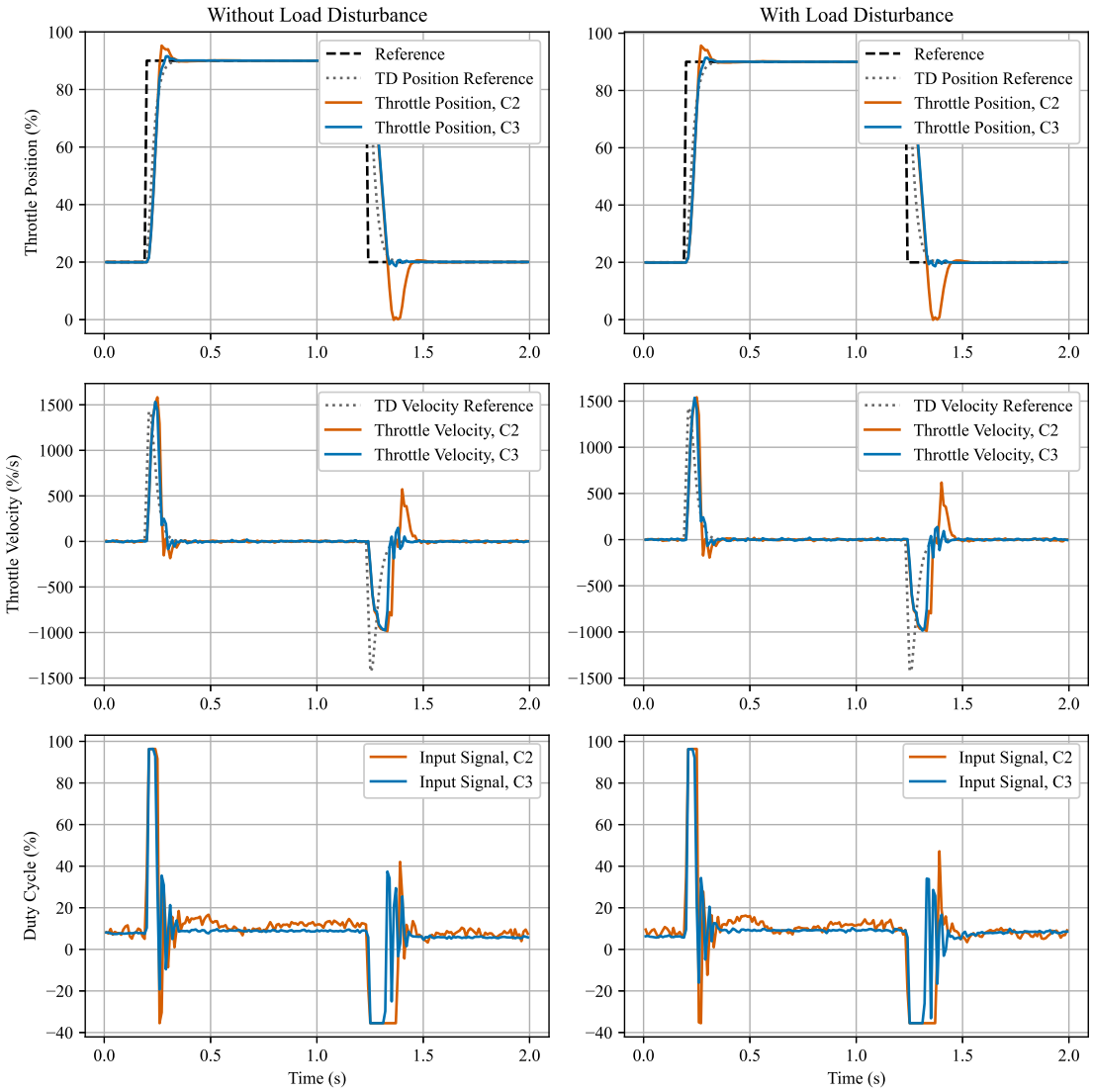

Figure 4.14: Comparison of Impulse Response between 20% and 90% of ADRC Controllers C2 and C3, with and without Load Disturbance

4.2.3 Real-Time Implementation of Feedforward Friction Compensation in PD Control on ECU

In this section there is a comparison between the nonlinear ADRC, the feedforward controller and T-Engineering's controller. The experiments will be the same as those previously evaluated.

The first experiment is a step responses from 20% to 30%, which can be observed in Figure 4.15. A 10% duty cycle decrement is made to the final control signal before the step in the right column of the figure to represent a load disturbance to the system.

When looking at the left column without load disturbance it is observed that all controllers perform similar to each other with the feedforward controller slightly faster than the other two. The step with the load disturbance in the right column we see that both the feedforward and ADRC performs similar to before while T-PID more than doubled the rise time, which can be seen in Table 4.1.

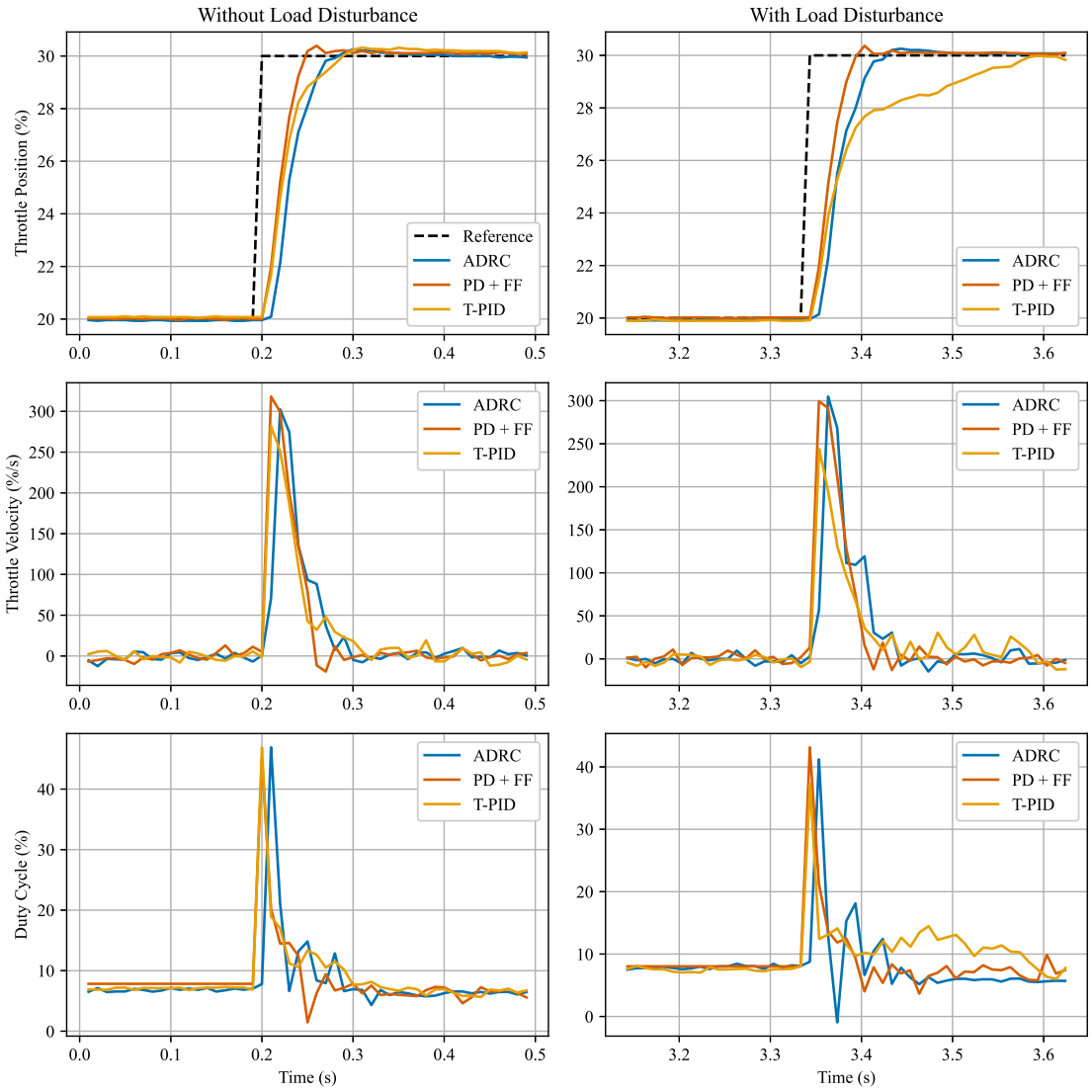

Figure 4.15: Comparison of Step Response between 20% and 30% of the three controllers, with and without Load Disturbance

The low-velocity tracking performance and the controllers ability to handle the full operating range are evaluated in Figure 4.16 for all controllers using a ramping reference from LHP up to 100%, and back down to LHP.

In Table 4.3 it is shown that the feedforward controller has a significantly lower MSE than the other two controllers, but with the cost of a higher control activity. It can also be observed that the MSE for the ADRC with the TD reference is lower than the T-PID MSE to the actual reference. But since the TD is slightly offset from the reference there is no way that the ADRC can get lower MSE than the other two controllers even if the MSE to TD reference would be 0.

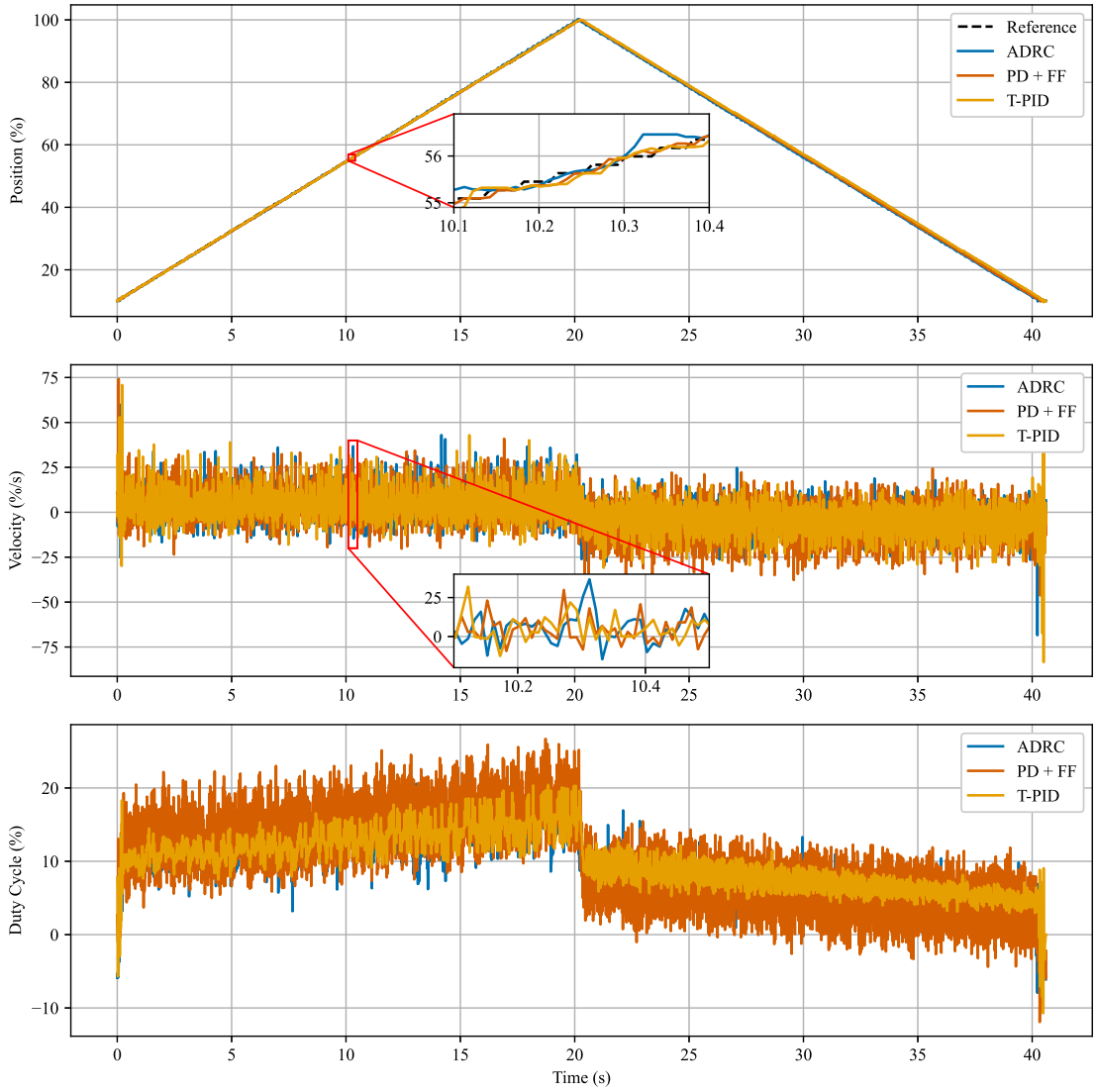

Figure 4.16: Comparison of the three controllers, Response for Ramping Input (LHP-100-LHP)

The low-velocity tracking performance and the controllers disturbance rejection ability is evaluated for all controllers using a low frequency sine wave from 20% to 70% in Figure 4.17. A load disturbance is applied to the final control signal according to the figure.

In Table 4.4 it is observed that the feedforward and T-PID performs similar in the MSE to the reference, while the feedforward has a much higher control activity. Just as the previous experiment, the ADRC has a higher MSE to the reference due to that the TD reference is slightly delayed, nonetheless the ADRC has the lowest controll activity of them all.

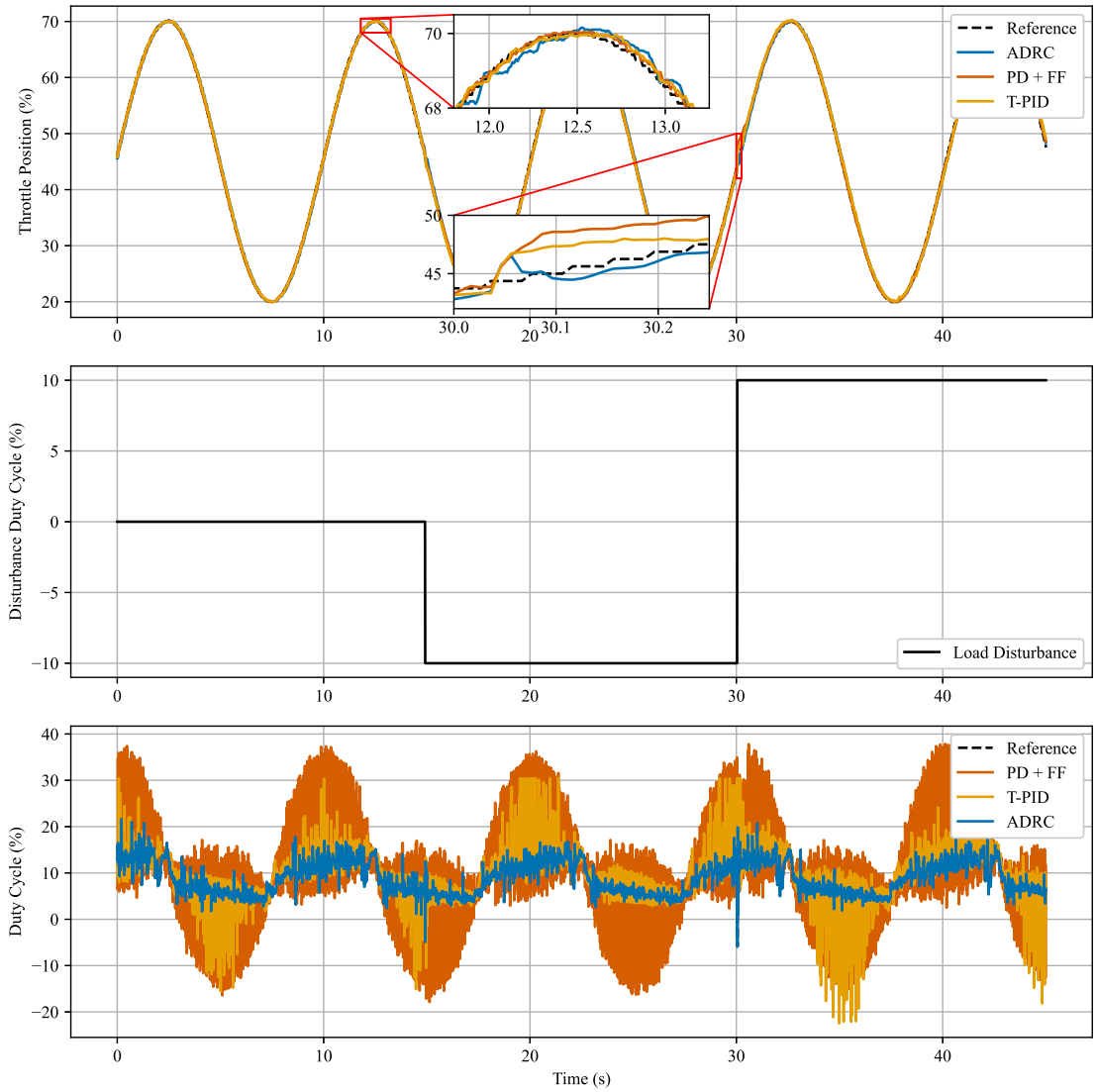

Figure 4.17: Comparison of the three controllers, Sine Wave tracking with Load Disturbance added

The controllers performance across the operating range is evaluated by applying a reference impulse between 20% and 90%, as shown in Figure 4.18. A load disturbance of −10% duty cycle is applied to the final control signal before the reference impulse shown in the right column of the figure.

In Table 4.2 it is observed that the ADRC and feedforward has a similar step response to each other while they both are faster than the T-PID. It is also shown in the table that the load disturbance doesn't effect the performance of the ADRC or feedforward while the T-PID gets a higher rise time.

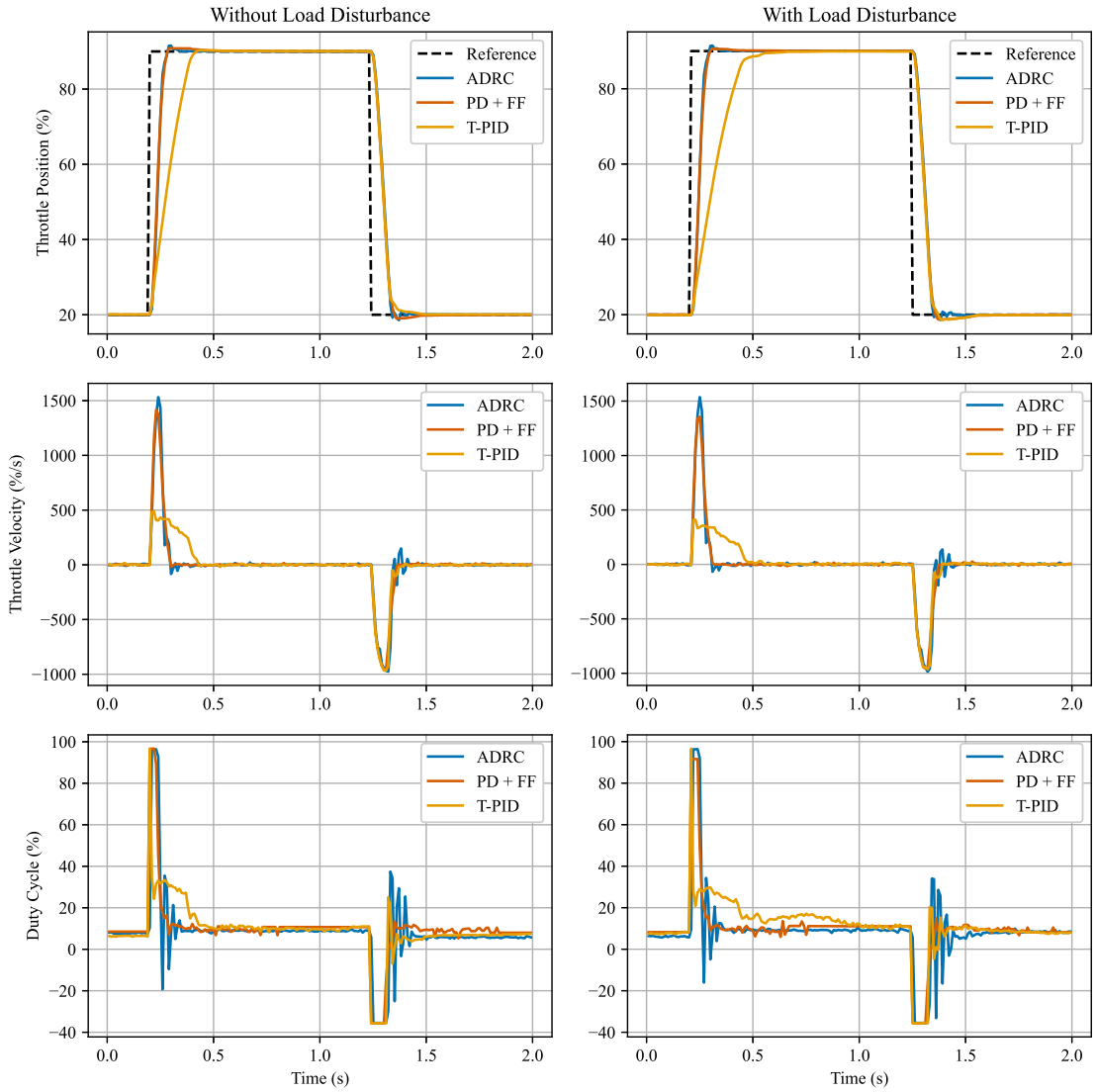

Figure 4.18: Comparison of Impulse Response between 20% and 90% of the three controllers, with and without Load Disturbance

4.2.4 Metrics from experiments

Here below is the following results from each experiment that is made to distinguish the different characteristics between each controller.

4.2.4.1 Step from 20% to 30% and Impulse between 20% and 90%

The rise times and angle of overshoot for the different controllers where measured during reference steps from 20% to 30% and are summarized in Table 4.1. It can be observed that the different controllers perform very comparable in both rise time and overshoot, with the Feedforward compensation and PD controller (PD+FF) performing much quicker because of its phase lead compensation during these small time frames. In this reference step experiment, a load disturbance was introduced by applying a constant offset of -10% to the final control signal one second before the reference step, allowing the controller to settle prior to the step change. This seemingly had no effect on any of the controllers but the controller T-PID. Because of its integral action, it adjusted to compensate for the disturbance. The PD+FF controller does not include integral action, so it avoids issues like integral windup. Instead steady-state errors are compensated for by the friction compensation feedforward, this eliminates the need for integral action in the controller. The ADRC has integral action in the sense that the disturbance is estimated and compensated for, and it happens quickly because of the high gain observer. Also, it is separate to the controller, not affecting rise time or tracking performance.

Controller	**Without Load Disturbance**		**With Load Disturbance**	
	Rise Time (0%-95%)	Overshoot	Rise Time (0%-95%)	Overshoot
LADRC C1	68 ms	0.24%	69 ms	0.24%
LADRC C2	69 ms	0.39%	68 ms	0.42%
NLADRC C3	66 ms	0.25%	66 ms	0.25%
PD + FF	43 ms	0.39%	46 ms	0.36%
T-PID	74 ms	0.32%	199 ms	0.00%

Table 4.1: Controller Performance Comparison for a Reference Step from 20% to 30%

A summary of rise times and angle of overshoot is presented in Table 4.2, measured during reference steps from 20% to 90%. These show that the controllers used in this thesis are much faster than that of the baseline controller T-PID. As the controllers where tuned to be as fast as T-PID during the smaller reference steps, the gains improved rise times in the greater step across the operating range. It also shows that the gains of the controllers can be relaxed to be comparable to the rise time of the T-PID controller, still passing performance requirements but instead improving control signal activity and thus actuator longevity. A moderate amount of overshoot can be observed from the linear ADRC controllers, indicating the controller gains are too high for reference changes across a wider range. It can also be observed in Figure 4.10 that the undershoot of the controllers when the reference is changed

from 90% to 20% is even greater than the angle of overshoot, further indicating that the decreased gains for high errors in the nonlinear ADRC was necessary for control of the system.

Controller	Without Load Disturbance		With Load Disturbance	
	Rise Time (0%-95%)	Overshoot	Rise Time (0%-95%)	Overshoot
LADRC C1	66 ms	4.65%	66 ms	6.03%
LADRC C2	67 ms	5.26%	67 ms	5.66%
NLADRC C3	76 ms	1.55%	77 ms	1.45%
PD + FF	80 ms	0.93%	83 ms	0.67%
T-PID	193 ms	0.29%	245 ms	0%

Table 4.2: Controller Performance Comparison for a Reference Step from 20% to 90%

4.2.4.2 Ramping and sinusoidal experiments

Tables 4.3 and 4.4 include tracking performance of low velocity reference changes, capturing the friction compensation. It shows the controller performance as mean squared Error (MSE) to the reference. It can be observed that all friction compensation methods offer a reduction in MSE to the uncompensated case. For the ADRC controllers, the MSE to the reference position generated by the TD is also measured. Because the TD creates a phase lag between the original reference and the generated reference signal, there is a constant offset between the original reference signal and the system's position. Its therefore important to study the value of the MSE to TD, to better understand the results of the friction compensation. In Table 4.4 it is especially important to carefully consider this, as the MSE of the ADRC controllers seemingly increases from the uncompensated case, when in fact, the controllers are following their generated reference with $9--30$ times lower MSE than the uncompensated controller. In Table 4.3, the performance of the controller's friction compensation during reference ramping can be seen. All controllers show clear results of friction compensation, Figure 4.5 and Figure 4.6 also show the effects of stick slip motion caused by friction when no friction compensation is used.

Controller	MSE to Ref.	MSE to TD Ref.	Input Variance
no Compensation	0.1102	N/A	13.54
LADRC C1	0.0362	0.0023	44.10
LADRC C2	0.0387	0.0045	14.90
NLADRC C3	0.0538	0.0152	13.30
PD + FF	0.0088	N/A	29.09
T-PID	0.0281	N/A	14.00

Table 4.3: Controller Performance Comparison During Ramping Input (LHP $\rightarrow$ 100% $\rightarrow$ LHP)

Controller	MSE to Ref.	MSE to TD Ref.	Input Variance
no Compensation	0.1812	N/A	29.53
LADRC C1	0.2279	0.0060	47.67
LADRC C2	0.2327	0.0109	14.94
NLADRC C3	0.2218	0.0201	11.58
PD + FF	0.1017	N/A	88.21
T-PID	0.1273	N/A	29.35

Table 4.4: Controller Performance Comparison During Sine Wave Tracking

4.2.4.3 Control Signal Activity

It can be observed from figures 4.16 and 4.17, and tables 4.3 and 4.4, where the controllers are compared in the reference ramping and sine wave experiments, that better performing friction compensation results in added control signal activity. It can especially be seen that the ADRC controller C1 has high control signal noise even when the reference is steady, resulting in unnecessary actuator wear, this was also greatly reduced with the addition of the nonlinear controller gain of the ADRC controller C3.

5
Conclusion

In this section, the project aim will be revisited and it will be demonstrated how the work presented in the methodology and results has addressed the stated objectives. The aim is to show that the project has fulfilled its intended purpose by linking the experimental findings and analysis to the original research goals.

5.1 Research Question

The primary objective of this thesis was to investigate the key characteristics that differentiate the performance of different friction models and friction compensation methods when applied to a real-time controller.

In this study, a PD controller with a LuGre friction compensation was implemented in a feedforward configuration. Additionally, a PD controller incorporating a model-free adaptive friction compensation was employed in the ADRC framework. The fundamental distinction between these approaches lies in the direct compensation of friction in the feedforward method, as opposed to the ADRC controller, which requires an intermediate estimation of friction prior to compensation.

The findings demonstrate a significant benefit of friction compensation in systems characterized by high static friction, leading to improved tracking performance. However, this improvement is accompanied by increased variance in the control signal. Notably, the application of a nonlinear control gain was shown to mitigate this variance, thereby potentially extending the operational lifespan of the system hardware.

5.2 Summary of Research

The motivation behind this research was to assess the extent to which friction compensation enhances controller performance and the difference between static and estimated friction compensation.

Overall, the experimental outcomes align with initial expectations, confirming that both static and estimated friction compensation facilitates rapid reference tracking without introducing overshoot.

The methodology used in this study proved effective. However, future implementations could benefit from an initial evaluation of the system's static friction characteristics, which would enable the exclusion of friction models that do not account

for static friction and streamline the analysis.

5.3 Future Work

Several avenues for future research are proposed. First, it would be valuable to investigate a feedforward friction compensation strategy in which the compensation parameters are gradually updated over time, thereby enhancing robustness to frictional variations. Second, further study is warranted to examine the performance of both adaptive and non-adaptive friction compensation schemes under conditions of varying friction. Finally, while this thesis explored the use of nonlinear control gains within the ADRC controller, future work could explore the implementation of nonlinear gains within the feedforward compensation to reduce control effort while maintaining performance.

5.4 Contributions to the Field

This thesis has demonstrated that adaptive friction compensation performs comparably to non-adaptive compensation under conditions of unchanging friction. This result highlights the substantial potential of ADRC for systems exhibiting significant static friction, offering a promising direction for improving control performance in such environments.

Bibliography

[1] Brian Armstrong-Hélouvry, Pierre Dupont, and Carlos Canudas De Wit. A survey of models, analysis tools and compensation methods for the control of machines with friction. *Automatica*, 30(7):1083–1138, 1994.

[2] Xiao Benxian, Wang Ping, Dong Xueping, Zhang Xingpeng, and Yu Haibin. Study on nonlinear friction compensation for bi-axis servo system based-on adrc. In *International Conference on Information Science and Technology*, pages 788–793. IEEE, 2011.

[3] C. Canudas, K. Astrom, and K. Braun. Adaptive friction compensation in dc-motor drives. *IEEE Journal on Robotics and Automation*, 3(6):681–685, 1987.

[4] C. Canudas de Wit, H. Olsson, K.J. Astrom, and P. Lischinsky. A new model for control of systems with friction. *IEEE Transactions on Automatic Control*, 40(3):419–425, 1995.

[5] Yunfeng Hu, Qifang Liu, Pengyuan Sun, Hong Chen, and Jun Li. Design of an adrc-based electronic throttle controller. In *Proceedings of the 30th Chinese Control Conference*, pages 6340–6344, 2011.

[6] D. Iles-Klumpner, I. Serban, and M. Risticevic. Automotive electrical actuation technologies. In *2006 IEEE Vehicle Power and Propulsion Conference*, pages 1–6, 2006.

[7] Ronald K Jurgen. *Electronic engine control technologies*. SAE International, 2004.

[8] R. N. Loh, W. Thanom, J. S. Pyko, and A. Lee. Electronic throttle control system: Modeling, identification and model-based control designs. *Engineering*, 5(07):589, 2013.

[9] C. Makkar, W.E. Dixon, W.G. Sawyer, and G. Hu. A new continuously differentiable friction model for control systems design. In *Proceedings, 2005 IEEE/ASME International Conference on Advanced Intelligent Mechatronics.*, pages 600–605, 2005.

[10] Henrik Olsson. *Control Systems with Friction*. Doctoral thesis (monograph), Department of Automatic Control, 1996. Defence details Date: 1996-05-24 Time: 10:15 Place: M-building M:A, Lund External reviewer(s) Name: Friedland, Bernard Title: Prof. Affiliation: New Jersey Institute of Technology —.

[11] Henrik Olsson, Karl Johan Åström, Carlos Canudas De Wit, Magnus Gäfvert, and Pablo Lischinsky. Friction models and friction compensation. *Eur. J. Control*, 4(3):176–195, 1998.

[12] Hans-Martin Streib and Hubert Bischof. Electronic throttle control (etc): A cost effective system for improved emissions, fuel economy, and driveability. In *SAE Technical Paper*, pages 1–10, International Congress & Exposition, 1996.

SAE International. Also in: Electronic Engine Control Technologies-PT-73, Electronic Engine Controls 1996-SP-1149.

[13] Dongxu Zhu, Xiaobo Qiu, Kai Wang, and Yongqiang Hou. Study on friction compensation for gun control system of tank based on adrc. In *2011 Second International Conference on Mechanic Automation and Control Engineering*, pages 1672–1675, 2011.

DEPARTMENT OF ELECTRICAL ENGINEERING
CHALMERS UNIVERSITY OF TECHNOLOGY
Gothenburg, Sweden
www.chalmers.se

CHALMERS
UNIVERSITY OF TECHNOLOGY